Cryogel scaffolds for regionally constrained delivery of lysophosphatidylcholine to central nervous system slice cultures: a model of focal demyelination for multiple sclerosis research

Dimitri Eigel[1†], Lida Zoupi[2†], Sowmya Sekizar[2†], Petra B. Welzel[1], Carsten Werner[1], Anna Williams[2*], Ben Newland[1,3*]

† these authors contributed equally

*anna.williams@ed.ac.uk

*newlandb@cardiff.ac.uk

1 - Leibniz-Institut für Polymerforschung Dresden e.V., Max Bergmann Center of Biomaterials Dresden, Hohe Straße 6, D-01069 Dresden, Germany

2 - MRC-Centre for Regenerative Medicine, University of Edinburgh, Edinburgh BioQuarter, 5 Little France Drive, EH16 4UU, Edinburgh, U.K.

3 - School of Pharmacy and Pharmaceutical Sciences, Cardiff University, Redwood Building, King Edward VII Avenue, Cardiff, CF10 3NB, U.K.

Keywords: remyelination, multiple sclerosis, cryogel, focal demyelination

Abstract

The pathology of multiple sclerosis (MS) is typified by focal demyelinated areas of the brain and spinal cord, which results in axonal degeneration and atrophy. Although the field has made much progress in developing immunomodulatory therapies to reduce the occurrence of these focal lesions, there is a conspicuous lack of licensed effective therapies to reduce axonal degeneration or promote repair. Remyelination, carried out by oligodendrocytes, does occur in MS, and is protective against axonal degeneration. Unfortunately, remyelination is not very efficient, and ultimately fails and so there is a research focus to generate new therapeutics to enhance remyelination leading to neuroprotection.

To develop these therapies, we need preclinical models that well reflect remyelination in MS. We have previously characterized an *ex vivo* model that uses lysophosphatidylcholine (LPC) to cause acute and global demyelination of tissue slices, followed by spontaneous remyelination, which has been widely used as a surrogate for *in vivo* rodent models of

demyelination. However, this *ex vivo* model lacks the focal demyelinated lesions seen in MS, surrounded by normal tissue from which the repairing oligodendrocytes are derived. Therefore, to improve the model, we have developed and characterized small macroporous cryogel scaffolds for controlled/regional delivery of LPC with diameters of either 0.5, 1 or 2 mm. Placement of LPC loaded scaffolds adjacent to *ex vivo* cultured mouse brain and spinal cord slices induced focal areas of demyelination in proximity to the scaffold. To the best of our knowledge, this is the first such report of spatial mimicry of the *in vivo* condition in *ex vivo* tissue culture. This will allow not only the investigation into focal lesions, but also provides a better platform technology with which to test remyelination-promoting therapeutics.

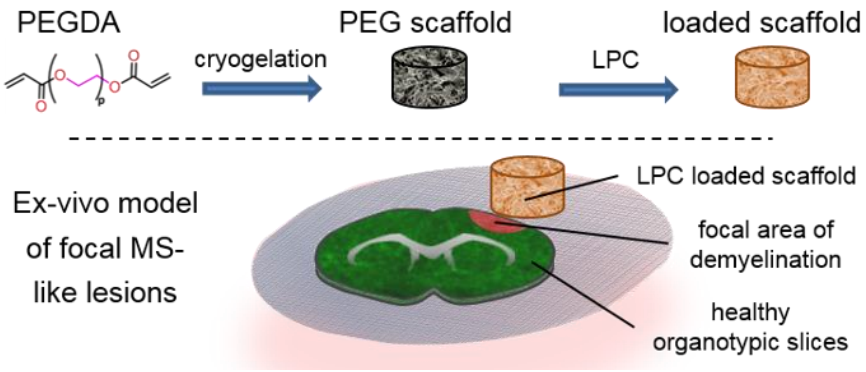

1 Introduction

Multiple sclerosis (MS) is an auto-immune and neurodegenerative disease causing focal areas of demyelination in the brain and spinal cord. It is the most common cause of non-traumatic neurological disability in young adults and affects around two million people worldwide [1, 2]. MS is a purely human disease, so, in order to study it, researchers have developed several models in other species. These various models capture different aspects of the disease, but no single model fully recapitulates the human condition (reviewed in [3]). With the help of the immune-driven models, where activated T cells drive demyelination, the research community has developed very successful immunomodulatory drugs which reduce the number of new MS lesions and symptomatic relapses in relapsing-remitting MS (reviewed in [4]). However, we are still far from a successful neuroprotective therapy which could slow, prevent or reverse accumulation of disability in progressive MS by reducing neurodegeneration. One strategy for neuroprotection is to encourage remyelination – where oligodendrocytes replace damaged myelin sheaths which restores saltatory nerve impulse conduction and provides metabolic support for the underlying axon [5]. Remyelination occurs

in MS but is inefficient and always ultimately fails [6, 7]. To test pro-remyelination compounds, different *in vivo* models have been developed to examine the remyelination response. *In vivo* toxin models aim to destroy white matter myelin in a focal way using stereotactic injections of lysolecithin (lysophosphatidylcholine, LPC) or both grey and white matter in a global manner using ingested cuprizone. The advantage of using LPC is that the location of the damage is known, demyelination and remyelination are separated and there is a well-characterized repair tempo [8, 9]. However, this is an *in vivo* model which is not suitable for high or even moderate throughput screening for pro-remyelinating therapeutics. For this reason, we previously characterized an *ex vivo* model of demyelination and remyelination using LPC applied to slices of brain and spinal cord grown in culture [10]. This technique, first introduced by Birgbauer et al., [11] involves the culture of 300 µm thick postnatal rodent brain slices and then demyelination of the whole slice, using LPC added to the culture medium. This has been very useful in screening compounds with relative ease, allowing selection of suitable compounds for further analysis *in vivo*. This model has been adopted throughout the myelin research community to test pro-remyelinating compounds [12-14], some of which have now entered clinical trials e.g. ClinicalTrials.gov Identifier: NCT03222973, EudraCT Number: 2014-003145-99. This method has the advantage of easy manipulation as drugs can be simply added to the culture medium.

Pro-remyelinating drugs may either increase the recruitment of the oligodendrocyte precursor cell (OPC) to a focal demyelinated MS lesion or to enhance the speed of OPC differentiation within this focal lesion into a remyelinating oligodendrocyte [5]. These appear to be critical steps in enhancing remyelination, as around 60% of post mortem MS demyelinated lesions contain OPCs apparently stalled in differentiation and in the remaining 30%, there is a low number of OPCs, suggesting a lack of recruitment from surrounding normal appearing “healthy” tissue [15]. A focal area of demyelination leads to locally-generated chemotactic cues forming a gradient of signals for cells to respond to, which is absent after global demyelination [8, 16, 17]. Our current system of global demyelination does not reflect the focal lesions of demyelination, surrounded by normal appearing white and grey matter found in MS, so we cannot test drugs enhancing recruitment, as there is no normal tissue from which to recruit from. To rectify this problem, and provide a better preclinical *ex vivo* model, we set out to generate and characterize a model of focal demyelination in rodent brain

and spinal cord slice cultures, using biomaterial scaffolds to deliver LPC to only one area of the tissue slice rather than to the whole tissue.

One such group of biomaterial scaffolds that has been extensively investigated as drug delivery systems in tissue engineering and regenerative medicine are hydrogels based on poly(ethylene glycol) [18-22]. They are chemically cross-linked and water-insoluble three-dimensional hydrophilic polymer networks. They are generally non-toxic/non-immunogenic, and have high small molecule permeability and mechanical properties that can be tailored to that of tissues. Hydrogels, however, have significant drawbacks for use in *ex-vivo* cultures [23, 24] as they dehydrate quickly and lose their shape when they are not permanently covered or exposed to aqueous conditions. Additionally, when they are transferred into their swollen state, hydrogels exhibit low mechanical stability and thus can become difficult to move/handle. Consequently, controlling the loading and delivery of drugs from such gels is challenging. An alternative biomaterial, also based on poly(ethylene glycol) starting materials, involves the chemical crosslinking of the monomeric precursor solution under freezing conditions. The resulting materials, termed cryogelated hydrogels (or cryogels) typically exhibit macroporous structures that are highly interconnected, with mechanically strong struts and stiff pore walls [25-27]. Cryogels exhibit high mechanical deformability without being destroyed and have remarkable shape memory with additional reversible and fast-swelling properties [28-30]. These beneficial features motivated us to investigate their use as an easy-to-handle scaffold for delivery of LPC focally to brain slice cultures.

2 Materials and Methods

2.1 Materials

All chemicals and consumables were used as received unless otherwise stated. Poly(ethylene glycol) diacrylate (PEGDA) (M_n = 700 g/mol), 2-hydroxy-2-methylpropiophenone (HMPP), phosphate buffered saline (PBS), bovine serum albumin (BSA), absolute ethanol (EtOH) and Corning Costar TC-treated multiple size 6 well plates were purchased from Sigma-Aldrich (St. Louis, MO, USA). Two types of LPC were used for these studies: the “standard” LPC used for the *ex vivo* studies (Sigma, L1381) and the fluorescent analogue 1-(dipyrrometheneboron difluoride)undecanoyl-2-hydroxy-*sn*-glycero-3-phosphocholine (TopFluor®Lyso PC) (Sigma, 810284P). ATTO 647-labeled maleimide was obtained from ATTO-TEC (Siegen, Germany).

Hydrophilic PTFE cell culture inserts with a diameter of 30 mm and a pore size of 0.4 µm were purchased from Merck Millipore (Darmstadt, Germany). Polystyrene templates with 0.5 mm, 1mm and 2 mm diameter cavities were self-made. All water used was highly purified and deionized using a Milli-Q® ('ultrapure' water of "Type 1") integral water purification system from Merck Millipore (Darmstadt, Germany).

2.2 Synthesis of macroporous cylindrical cryogels

The cylindrical cryogels were synthesized in polystyrene templates via photochemical crosslinking. The templates were created by drilling 0.5 mm, 1 mm or 2 mm holes through a polystyrene sheet (Evergreen Scale Models, USA) of different thickness (0.5 mm, 0.7 mm or 1.5 mm respectively, as reported by the manufacturer). One side of the template was covered by Scotch Magic™ Tape (3M, Maplewood, Minnesota, U.S.A.) to cover the hole, thus creating a cavity in which the cryogels are be synthesized. An aqueous precursor solution was freshly prepared prior to use, containing 70 mg/mL PEGDA monomer and 10 mg/mL HMPP as a photoinitiator. 0.13 µL, 0.78 µL or 5.02 µL of this solution were added to the respective cavities. The filled templates were then placed in the freezer for 30 minutes at a processing temperature of -20°C. Then, each template was exposed to UV light (8 W UV hand lamp, wavelength 254 nm, Benda, Wiesloch, Germany) for 3 minutes whilst still at -20°C. The resulting cylindrical cryogels were removed from their template and washed two times with absolute ethanol and two times with Milli-Q in order to remove unbound monomers or photoinitiator. Finally, the cryogels were left to dry for 5 hours in a vacuum at room temperature.

2.3 Template characterization by multi-pinhole confocal microscopy

The dimensions and the topography of the empty and cryogel filled polystyrene templates were analyzed via multi-pinhole confocal microscopy utilizing a µsurf explorer (NanoFocus AG, Germany) equipped with a 10x objective (Olympus, Germany). 2D and 3D height maps were generated, and profile sections were recorded using µSoft analysis software (NanoFocus AG).

2.4 Cryogel characterization by Raman spectroscopy

The Raman spectra of the cylindrical cryogels were recorded and baseline corrected with the Raman Imaging System alpha300R (WITEC, Ulm, Germany) in the 600–1900 cm^{-1} frequency range (excitation wavelength: 785 nm, laser power: 130 mW, objective: 20x (Zeiss), integration time: 0.5 s, accumulation per spectrum: 200). The spectra of the PEGDA monomer solution and the precursor solution, which contained the monomer and photoinitiator, were used as references.

2.5 Cryogel characterization by Fourier transform infrared spectroscopy (FTIR)

Infrared spectra of the cylindrical cryogels were obtained and baseline corrected using a Bruker Vertex 80v (Billerica, USA) equipped with a Golden Gate™ single reflection diamond attenuated total reflectance probe (ATR) system from SPECAC (Orpington, U.K.) in the 600–4000 cm^{-1} frequency range (MCT-detector, resolution = 4 cm^{-1}, 100 scans per measurement). The spectrum of the PEGDA monomer was used as a reference.

2.6 Scanning electron microscopy analysis of the cryogels (SEM)

Surface and pore morphological features of the cylindrical cryogels were visualized by means of a XL30 ESEM-FEG microscope (Philips, Netherlands) in high vacuum mode using an accelerating voltage of 7.5 kV. Samples were fixed to aluminum stubs with double-sided adhesive carbon conductive tape and subsequently sputter-coated with gold using a SCD 050 sputter coater (BAL-TEC, Germany) for 40 s at 40 mA.

2.7 Swelling measurements

Swelling studies were carried out in PBS (pH 7.4) containing 1% (w/v) BSA at room temperature (23 °C). Before swelling, the dry cryogels were scanned with the fluorescent image analyzer FLA-5000 (Fujifilm, Japan) and the average diameter was measured for every cylinder by a three-point determination method using the Multi Gauge analysis software (Fujifilm, Japan). Afterwards, the cylindrical cryogels were immersed in 2 mL of the buffer containing BSA for 24 hours at room temperature until the equilibrium was reached. The final diameter of the swollen cryogels was measured immediately after the removal of excess buffer from the cryogel surface. At least six independent experiments were carried out (n = 6). The volume swelling degree Qv for the cryogels was obtained from the diameter of the swollen d and the dry cryogel d_0 via equation (1)

$$Q_v = \left(\frac{d}{d_0}\right)^3 \quad (1)$$

2.8 Pore size analysis via confocal laser scanning microscopy (CLSM)

CLSM was used to visualize and measure the pore size of the cylindrical cryogels in the hydrated state (in PBS). Therefore, the cryogels were labeled by adding 0.1 mg/mL of ATTO 647-labeled maleimide to the precursor solution, followed by a subsequent photochemical crosslinking analogously to the cryogel synthesis. CLSM was performed with a Dragonfly (Andor Technology, U.K.) mounted on a Nikon Ti-E inverted microscope with a 637 nm laser and diode and images were taken with either a 10x magnification objective (CFI Plan Apo Lambda, Nikon), or a 20x magnification objective (CFI Plan Apo Lambda, Nikon). Pore sizes were analyzed from 15 images taken from 8 different z-planes with a distance of 2.3 µm between each plane, measuring a total of 300 pores in both x- and y-directions using ImageJ software (NIH). The surface area of the pores was analyzed using algorithm functions of the ImageJ software. The pore volume analysis was performed using Imaris software v. 9.30 (Bitplane AG, Zurich, Switzerland). The software's built-in wizard was used to perform a surface reconstruction function, which enabled calculation of the volume of interest from a newly generated surface object. The porosity was calculated from the ratio of pore volume to the total cryogel cylinder volume.

2.9 Compression rheology

Uniaxial compression tests were performed on 9 mm diameter and 3 mm height PBS swollen cylindrical cryogels at room temperature under atmospheric conditions by using an ARES G2 Rheometer (TA Instruments, New Castle, DE, U.S.A.). Samples were compressed between two parallel plates (stainless steel, diameter 8 mm) with a constant linear compression rate of 1 mm/min. The compressive modulus (E) of the cryogels was calculated via equation (2) using the uniaxial stress (σ) and strain (ϵ) parameters from the linear region of the compression curves at low strain regions (0−5% up to 25%) that were obtained through ten independently performed experiments.

$$E = \frac{\Delta\sigma}{\Delta\epsilon} \quad (2)$$

2.10 Lysophosphatidylcholine (LPC) loading and release analysis

The LPC loading and release analysis was performed by using TopFluor®Lyso PC, a fluorescently labeled LPC analogue. The LPC was first dissolved in sterile phosphate buffered saline (PBS) at a concentration of 10 mg/mL (termed the loading stock solution) and the cylindrical cryogels (n = 4 for each diameter type) were subsequently incubated in 100 µL of this solution for 5 minutes at 37°C. After the incubation time, the LPC soaked cryogels were carefully blotted with a lint-free tissue in order to remove the excess and thus unbound LPC. Afterwards, the cryogels were immediately placed individually on 30 mm diameter PTFE cell culture inserts (0.4 µm pore size) in six-well plates with 1 mL of fresh brain slice medium underneath. This is to mimic the situation where these are applied to cultured tissue slices. The amount of LPC loaded was determined by measuring the volume of the remaining loading stock solution and subtracting this from the initial volume of 100 µL.

To determine whether additional LPC was depleted from the loading solution by the cryogel (i.e. determine if electrostatic loading was taking place) the fluorescence intensity of the remaining incubation volume was measured in comparison to an equal volume of the LPC loading stock solution that was not used for incubation.

To measure how much LPC was released from the cryogel to the medium under the insert, 200 µL of the undernatant was removed and replaced with fresh slice medium at each time point (incubated at 37 °C). The collected volumes were stored at – 80 °C until analyzed fluorometrically using a microplate reader Spark® (Tecan Trading AG, Switzerland, excitation wavelength λ_{exc} = 477 nm and emission wavelength λ_{em} = 527 nm) in comparison to a standard curve. The amount of LPC removed for each time point was factored into the calculation of total LPC release.

2.11 Slice cultures

All animal experiments were carried out in line with UK Home Office guidelines, under project license 60/4524 (A.W.). LPC used for these studies was not fluorescently labelled (Sigma, L1381).

Spinal Cord Slices

P0-P2 C57BL6/N mouse pups were decapitated and cervical spinal cord (about 3mm in length) was collected in ice cold L-15 (Life Technologies, 11415049). Meninges and blood vessels were

removed using fine forceps and the spinal cord was cut into 300 µm longitudinal slices, using a tissue chopper (McIlwain). Spinal cord slices were collected using a bent spatula into warmed slice medium consisting of 50% MEM (Invitrogen, 32360-026) with 25% Earle's Balanced Salt Solution (Invitrogen, 24010-043), 25% heat-inactivated horse serum (Invitrogen, 26050-088), 1% glutamax supplement (Invitrogen, 35050-038), 1% penicillin–streptomycin, 0.5% Fungizone (Invitrogen, 15290-018) and 6.5 mg/ml glucose (Sigma G8769). Slices were separated using blunt scalpels or needles. Separated slices were placed onto Millicell cell culture inserts which are placed in a six-well plate and have 1 mL slice culture medium underneath the insert. These air-liquid interface slice cultures were cultured for 15-20 days with medium changes every 2 days at 37 °C and 7.5% CO_2. For focal demyelination, 0.5 mm cryogels were soaked in 10 mg/mL LPC in PBS for 5 minutes. These were then placed adjacent to spinal cord slices (using forceps) but not in direct contact with slice (photographs were taken to help locate the site of lesion when processed for immune labelling). Cryogels were removed after 16 hrs (as optimized previously [10]) and the medium changed. Slices were fixed at desired time points for immunostaining. The day of the cryogel placement was considered as day 0. Day 3 was considered the time-point for maximal demyelination and day 14 the time-point for remyelination when the slices were processed for immunofluorescent labelling. For the control group, slice saline-soaked cryogels were placed adjacent to the spinal cord slices on Day 0 and removed 16hrs later.

Cortical Slices

P2–P3 C57BL6/N mouse pups were decapitated and their brains were dissected in cold Hibernate-A medium (Thermo Fisher A12475-01) on ice. Subsequently the brains were mounted on a vibratome (Leica) and 300 µm coronal cortical slices were collected in ice cold Hibernate-A medium. The slices were immediately transferred onto Millicell cell culture inserts (30 mm, hydrophilic PTFE, 0.4 µm, Merck-Millipore, PICM0RG50) using a bent spatula and in medium (composition as described in spinal cord slices). The slices were kept in culture for 16 days at 37 °C and 7.5% CO_2. The medium was changed every other day. Focal demyelination of the cortex was obtained by soaking 2.0 mm cryogels in 10 mg/ml of LPC and by placing them adjacent to the cortex for 16 hrs (as optimized previously [10]). The bigger cryogel size was found to be more effective for the larger cortical slices. For the control group, saline-soaked cryogels were placed adjacent to the cortical slices for 16 hours and then

removed. After this period, the cryogels were removed and the medium was replaced. The day of the LPC-cryogel placement was considered as day 0. Day 5 was considered the time-point for maximal demyelination and day 14 the time-point for remyelination when the slices were processed for immunofluorescent labelling.

Multiple tissue slices can be placed on each Millicell insert in a six well plate. As cortical slices are rather large, we suggest placing no more than 4 on an insert. Spinal cord slices are smaller and so 5 can be placed on an insert. Use of more than this number per insert risks that LPC loaded into the multiple cryogels releases too much LPC into the underlying culture medium producing a global effect.

2.12 Slice culture immunofluorescence

Cortical and spinal cord slices were washed once with PBS before they were fixed with 4% paraformaldehyde (PFA) in PBS for 1 hr at RT. The slices were subsequently rinsed in PBS and blocked in 3% heat-inactivated horse serum (Invitrogen, 26050-088), 2% BSA (Sigma, A7906), and 0.5% Triton X-100 in PBS for 2 hrs at RT. Following blocking, the slices were incubated for 48 hrs with primary antibodies at 4 °C. The slices were then washed 3 times with blocking solution and incubated with the appropriate secondary antibodies overnight at 4 °C. Finally, the slices were washed in PBS, counterstained with Hoechst 33342 solution (Thermo Fisher Scientific, 62249) and mounted on a glass microscopic slide using Mowiol mounting medium (Merck Millipore, 475904). The primary antibodies used were as follows: against myelin basic protein (rat monoclonal anti-MBP, MCA409S, BioRad, 1:300), Neurofilament-H (chicken polyclonal anti-NF-H, Biolegend, 822601. 1:10.000), IBA-1 (rabbit polyclonal, Wako chemicals, 019-19741 1:500). Secondary antibodies were all purchased from Life Technologies (Alexa, 1:1000). Images were obtained using confocal laser scanning microscopy (Leica microsystems, TCS SP8) and processed using Fiji image processing package (https://imagej.net/Fiji).

2.13 Statistical analysis

All graphs shown means plus error bars that represent either +/- standard deviation or standard error of means as stated in the figure legend. Differences between groups were

analyzed using a one-way ANOVA with Tukey post-hoc test. Data were considered significant if *P<0.05, ** P<0.01, *** P<0.001 or ****P<0.0001. Numbers of animals used for each experiment is stated in each figure legend.

3 Results

3.1 Successful formation of cylindrical and macroporous PEGDA cryogels

PEGDA based cylindrical cryogel scaffolds were successfully synthesized by free radical photopolymerisation at a subzero processing temperature (-20 °C) in polystyrene template sheet cavities, exhibiting interconnecting macropores within their network structure (**Figure 1**).

The resulting dimensions of the three variations of the cryogel scaffolds were 0.49 x 0.68 mm (diameter x height), 0.88 x 0.92 mm and 1.80 x 1.60 mm as determined from the profile measurements, which were obtained by means of multi-pinhole confocal microscopy analysis (**Figure 2**, **Supporting Information Figures S1**, **S2** and **Table S1**). However, these are termed by their intended diameter henceforward as 0.5 mm, 1 mm and 2 mm respectively. In addition, the confocal multi-pinhole observations also showed the porous cryogel structure for all three different cylinder sizes, which completely filled the cavities without the appearance of a meniscus like shape or over fillings (**Figure 2A-D, Figures S1 A-D** and **Figure S2A-D)**.

3.2 *Cylindrical PEGDA cryogels exhibit a sponge-like morphology*

The morphological analysis was carried out using SEM and confocal laser scanning fluorescence microscopy (CLSM). From SEM observations, the PEGDA cryogels exhibited a compact structure of interconnected macropores with a heterogeneous sponge-like morphology (**Figure 3A-C** and **Supporting Information Figure S3A-F**). All scaffolds also appeared to have rather randomly shaped but evenly distributed lamellar-like pores within or on top of the sponge-like structure with no overall defects (**Figure S3A-F)**. Whilst SEM analysis was used to reveal the cryogel structure in the dehydrated state, CLSM was performed to study the pore structure under hydrated conditions (application relevant situation). It should be noted that the wavelength of UV light chosen for the photoinitiation (366 nm) did not photo-bleach the samples as the far-red (647 nm) ATTO dye was selected

for the cryogel functionalization. The ATTO functionalized cryogel cylinders were swollen in PBS and directly characterized. **Figure 3D-F** and **Supporting Figure S3G-I** reveal the macroporous structure of the cryogel samples in their hydrated state. It can be clearly seen that CSLM and SEM investigations show similar morphological characteristics. The 1 mm and 2 mm sized cryogel cylinders show a very similar pore size distribution ranging between 10 µm and 110 µm (**Figure 3G**) with average pore diameters of 40.5 µm and 48.3 µm respectively**.** By comparison, the 0.5 mm sized cryogel cylinders, have pore sizes that range between 1-60 µm (**Figure 3G**) and an average pore diameter of 16.4 µm (see **Table S1** for general porosity characteristics of the cryogels). In summary, SEM and CLSM studies confirmed that the three different cryogel sizes consist of a continuous, highly macroporous structure. This high porosity should provide a high surface area to volume ratio (**Table S1**) for

3.3 Raman and FTIR spectra analysis reveal a completely covalent network

Raman and FTIR spectroscopy analysis were performed as complementary methods on the cylindrical PEGDA cryogels in comparison to the monomer and precursor solution. These two methods allow the confirmation of successful photoinitiated crosslinking of the PEGDA in the resulting cryogel scaffolds after UV irradiation (**Figure S4** and **Figure S5**). Both spectral analyses confirmed the absence of characteristic vinyl C=C (1640 cm^{-1}, Raman; 1620-1635 cm^{-1}, FTIR) and vinyl CH_2 (1410 cm^{-1}, Raman; 810 cm^{-1} and 1410 cm^{-1}, FTIR) vibrations in the cryogel after the precursor solution was exposed to UV light for 3 minutes. In addition, the characteristic C=O vibration of the PEGDA ester groups (1723 cm^{-1}, Raman; 1723 cm^{-1}, FTIR) was reduced in intensity [31, 32] and shifted (1733 cm^{-1}, Raman; 1730 cm^{-1}, FTIR) after the crosslinking reaction was performed. These results provide the evidence of complete covalent bonding within the cryogel network and thus no free vinyl groups remain in the structure.

3.4 The cryogel specific sponge-like morphology allows fast and reversible swelling

The swelling properties of the three differently sized cylindrical PEGDA cryogels are shown in **Figure S6**. Due to their open sponge-like structure, which shows a high surface area to volume ratio (**Table S1**), water or other solvents can easily absorb into the cryogel cylinders through the interconnected pore structure of the scaffold. The swelling equilibrium of the different cryogels was reached within a few minutes, whereby an opaque appearance is obtained (related to the heterogeneous pore structure of the cryogels). The calculated volume swelling

degrees of the differently sized cryogels are, as expected, almost identical because they all consist of the same crosslinked material (PEGDA 700). In general, all three cylindrical cryogels can also simply be dried and stored under dry state conditions and re-swollen at any time as required.

3.5 Cylindrical PEGDA cryogels can withstand high compressive stress

The mechanical properties of the cryogels were analyzed by a compression test. The **Figure S7** shows uniaxial compression stress-strain curves obtained for the cylindrical PEGDA cryogels, which has also been reported for other types of cryogel material [25, 28, 33]. The curve shape of the compression measurements follows an initial weak stress-strain response, which turns into a dramatic stress increase when higher strains are applied. The cylindrical PEGDA cryogels could withstand compression strain of 90% (up to about 160 kPa) without any cracks or destruction. Additionally, after a complete compression test, the cryogels could be easily regenerated to their original shape when immersed in PBS. In order to estimate the mechanical strength and elasticity of the cryogels, the average Young's modulus (*5 ± 0.5 kPa*) was determined from the slope of the stress-strain curves (eq. (2)). Such rather low Young's modulus demonstrates the elastic and spongy nature of these cryogel scaffolds, which provides them with appropriate physical property for applications in neuronal tissue engineering [34].

3.6 Scaffolds loaded with LPC show minimal global release to the culture medium

Figure 4A and 4B show a schematic representation of the proposed interactions between LPC and the cryogels, with a color change being noted due to the intense orange color of the fluorescently labelled LPC analogue used for this analysis (**Figure 4C**). There was no depletion of LPC concentration from the loading solution (**Figure 4D**), showing that loading to the cryogel scaffolds was simply by filling the swelled volume like a sponge with total amount of LPC loading being dependent on cryogel size **(Figure 4E** and **Figure S8)**. To determine the rate of LPC release to the medium below the culture insert, samples of the medium were analyzed for up to 16 hours of incubation. **Figure 4F** shows that different release profiles were obtained for differently sized cryogel cylinders. A plateau was reached for the 0.5 mm cryogels, but a greater amount of LPC was released from the larger cryogels with an almost linear release behavior from the 2 mm cryogels.

3.7 Cryogels induce focal demyelination of central nervous system slices

LPC- or control medium-loaded cryogels were placed next to CNS slices for 16 hrs (as previously optimized [10]), using 2 mm diameter cryogels for cortical slices and 0.5 mm diameter cryogels for the smaller spinal cord slices **(Figure 5A-D)**. These tissue areas were chosen to have either white matter (spinal cord) or grey matter (cortical) at the edge of the slice so that focal demyelination in both areas was possible from LPC diffusing in from the slice edge. These coronal brain slices or longitudinal spinal cord slices from new-born, wild type mice were allowed to myelinate in culture more than 2 weeks **(Figure 5A-D),** and immunofluorescence for myelin basic protein (MBP) was used as an indicator of the extent of myelination **(Figure 5B,C).**

3.8 White matter demyelination

0.5 mm LPC-loaded or saline loaded (control) cryogels were placed adjacent to longitudinal spinal cord sections, and the area close to the cryogel was compared to a distant area (unaffected) of the spinal cord **(Figure 6, Figure S9A,B)**. Control cryogels induced no demyelination at either day 3 or day 14 (as expected) **(Figure 6A)**. However, LPC loaded cryogels caused demyelination adjacent to the position of the cryogel which could be observed by a loss of MBP immunofluorescence staining at day 3 **(Figure 6B)**, reaching approximately 0.5 mm into the slice **(Figure 6C)** or 26% of the spinal cord area. More myelin was lost within the lesion than at the perilesion area **(Figure 6C)**. Neurofilament (NF) labelling **(Figure 6B)**, showed that whilst demyelination had occurred, the axons had remained. As we would expect in response to demyelination, there is an invasion of the demyelinated area by IBA1+ microglia at this time-point as a mechanism to clear myelin debris **(Figure 6B)**. This is absent from the slices treated with control cryogels **(Figure 6A)**. From our work with global demyelination of CNS slices [10], and *in vivo* demyelination in the mouse [8], we would expect remyelination to occur by day 14. At this time-point, adjacent to the LPC-loaded cryogel position, myelin debris was absent and MBP+ myelin sheaths were visible again **(Figure 6B)** showing that remyelination had successfully occurred (quantified in **Figure 6D**). This demyelination and spontaneous remyelination occurred in a focal manner, with the distal region of the spinal cord not affected **(Figure 6C,D, Figure S9B)**.

3.9 Grey matter demyelination

To model grey matter demyelination in a focal manner, we tested the larger 2 mm cryogels placed adjacent to cultured coronal slices of mouse brain cortex, targeting the motor cortex **(Figure 7A,B and Figure S9C,D)**. Again, in contrast to slices treated with control cryogels, we saw focal areas of demyelination in the slices adjacent to the position of the cryogel, affecting the cortical layers I-V, reaching an extent of 0.4 mm **(Figure 7B)**. The myelin debris took longer to clear in the cortical slices than spinal cord slices, reaching a nadir at the later time point of 5 days **(Figure 7B,C)**. At day 5, there was a focal lack of MBP+ immunofluorescence after application of the LPC-loaded cryogel, normal axonal staining with NF antibodies and invasion of the demyelinated area by IBA1+ microglia **(Figure 7B)**. Perilesional areas had an intermediate amount of myelin, less than that on the contralateral side **(Figure 7C)**. At day 14, when we expect remyelination to have occurred, MBP+ myelin profiles returned, quantified in **(Figure 7D)** and the number of IBA1+ microglia reduced **(Figure 7B).** The contralateral hemisphere of the slice was not affected by the addition of the LPC-loaded cryogel **(Figure S9D)** showing that the action of the LPC was limited to the adjacent tissue area only (average lesion depth of 394 μm ±82 μm).

In both cases of focal demyelination, in spinal cord and cortex, similarly to after global demyelination[10], we were able to successfully immunolabel for other markers of oligodendroglia, paranodal structures and proliferating cells, showing the potential use of this model to answer a variety of different biological questions (illustrated in **Figures S10 and S11**).

4 Discussion

LPC is widely used in the myelin field as a myelin toxin, and can be injected into the nervous system to produce precise and localized areas of demyelination [35]. Addition of LPC to CNS slice cultures offers a practical alternative to the use of whole organisms for studying the demyelination and remyelination processes that take place during MS progression. However, studies to date have shown that addition of LPC to culture medium below the slice, inevitably creates a uniform global demyelination effect [8, 10], thus not representing the uneven nature of the disease pathology. Direct injection into the slice is impractical due to the thin

depth of tissue required for this culture method. Furthermore, previous attempts only resulted global demyelination across the slice.

In this research we sought a means of affecting only a small region of the tissue, leaving the rest in an unaltered, healthy condition. For this we proposed the use of macroporous cryogel scaffolds; their soft yet robust structure making them easy to handle and quick to soak up liquids like a sponge.

A non-degradable, poly(ethylene glycol) based material was chosen for the relative inert nature it exhibits towards brain tissue [36]. Photo-initiated free radical polymerization of poly(ethylene glycol) diacrylate was chosen for network formation due to the versatility that it allows in terms of defining the freezing schedule prior to, not during, the polymerization reaction. Unlike previous studies, where network formation (gelation) took place during the freezing process [33, 37-39], herein we could pre-determine the freezing parameters, then expose the monomer solution to ultraviolet light to initiate the reaction. Not only did this give good control over pore size **(Figure 3)**, but it was a quick production method, with high reaction efficiency (all vinyl groups reacted **Figure S4** and **Figure S5)**.

LPC loading to the cryogel scaffolds was achieved simply through filling the macropores and was therefore directly proportional to cryogel cylinder size (larger scaffolds were loaded with more LPC). Although hydrogen bond interactions between the hydroxide groups of the LPC and the various carbonyl functionalities of the network can take place, no depletion of the concentration of the loading solution was noticed (i.e. LPC is not being electrostatically drawn out of solution onto the scaffold). Since we hypothesized that cryogel scaffolds could be used to deliver LPC to CNS slices cultured on the air-liquid interface, we first wanted to analyze how the LPC would be released in such a set up. If too much LPC would be released to the medium instead of the neighboring tissue area, then no specific focal effect would be obtained, and global demyelination would result. It should be noted that in our study actually a very low total amount of LPC was effectively released from the PEG based cryogels, into the medium below the insert membrane (0.7 µg (0.5 mm cryogel), 5.1 µg (1 mm cryogel) and 12 µg (2 mm cryogel) (**Figure 4F**) in comparison to the total loading amount of 5 – 100 µg (**Figure S8**). This is far below the level required to create the global demyelination model (0.5 mg/mL)[10]. This was a very important finding, showing that the cryogel cylinders could potentially cause only focal demyelination in CNS slices rather than global demyelination of the whole tissue. In addition, due to the different loading and release profiles, we could

envisage that the different cryogel cylinder slices would be suitable for different tissue slice sizes (i.e. brain vs spinal cord). We therefore took advantage of these small cryogel cylinders to focally introduce LPC to different sized tissue slices (cortex and the spinal cord).

For white matter lesions we used longitudinal spinal cord slices that were first left to myelinate *ex vivo* for more than 2 weeks. In the spinal cord, the white matter is located around the outermost area, and so should be amenable to demyelination from an adjacent LPC-loaded cryogel. In contrast to our previous global demyelination [8, 10], a focal region of demyelination was created in proximity to the cryogel placement (day 3) which, after removal of the cryogel, subsequently became remyelinated by day 14.

Apart from the white matter pathology, there is now increasing evidence that in MS there is also demyelinating damage affecting grey matter areas where the neurons reside and that it correlates well with neurological disability [40, 41],[42-44]. We therefore wanted to see if LPC loaded cryogel scaffolds could be used to create specific grey matter lesions. If accomplished, this could allow researchers to analyze the effect of therapeutic strategies on both the white matter and grey matter individually. In that case the larger diameter cryogel scaffolds were used (2mm) for the larger cortical slices. Again, focal demyelination was achieved, this time after 5 days, and subsequent remyelination also occurred.

To the best of our knowledge, these are the first such examples of non-uniform or “patchy” MS-like pathology in a central nervous system culture. These results not only prove the concept that focal demyelination can be set up using *ex-vivo* slice cultures, but also highlight the versatility of the approach as a means of focal tissue manipulation in general. Future studies will now focus on the underlying processes occurring during remyelination and the interplay between the healthy and pathological tissue regions, including microglia and oligodendrocyte recruitment. We envisage that this will not only give us a better understanding of the disease process, but provide a better disease-mimicking model to testing new therapeutic compounds.

5 Conclusion

We have induced focal demyelination of white matter and grey matter areas of mouse brain and spinal cord slice *in vitro* MS models using PEG-based cryogels loaded with LPC. Similarly to in global demyelination of CNS slices, we see demyelination and microglial invasion, followed by remyelination. However, the novelty of these models is that the focal pathology

surrounded by healthy tissue allows the study of recruitment of OPCs to these lesions, an important factor in at least 30% of MS lesions. Understanding grey matter pathology in MS is considered of increasing importance in neurodegeneration and cognitive dysfunction, and in cortical slices we have induced focal grey matter lesions. Slice cultures are an ideal tool for studying remyelination as they allow easy addition of drugs/cells/small molecules aiming to influence remyelination, with live imaging possible, enabling screening of compounds *in vitro* at moderate throughput before testing *in vivo*. We also predict that these soft but robust cryogel scaffolds may also be useful in applying LPC or other drugs (toxins or therapeutics) *in vivo*.

This focal demyelinating *ex vivo* model represents a step forward in the tools available to improve understanding of CNS remyelination and to screen for pro-remyelination compounds, that may in the future be used in for therapies to help progressive MS.

Acknowledgements:

Funding: This work was supported by the MS Society UK, the MS International Federation and by the Deutsche Forschungsgemeinschaft (DFG) – Project number 320041273. The authors would like to thank Dieter Fischer and Mikhail Malanin for assistance with Raman and FTIR spectroscopy respectively.

Author Contributions:

BN and AW conceived the idea. DE, LZ, SS and BN performed the experiments and analysis. PW, AW, CW and BN critically analyzed the data and assisted in experimental design. All authors contributed to writing the manuscript.

Declaration of Interest:

The authors declare no conflicts of interest.

Data Availability:

Supplementary Information: Supplementary Figures S1-S8 and Table S1 available online

References

[1] Atlas of MS 2013: Mapping Multiple Sclerosis Around the World. In: Federation MSI, editor. London: http://www.msif.org/about-ms/publications-and-resources/; 2013.

[2] Atlas: Multiple Sclerosis Resources in the World 2008. In: Organization WH, editor. Geneva, Switzerland: http://www.msif.org/about-ms/publications-and-resources/; 2008.
[3] Kipp M, Nyamoya S, Hochstrasser T, Amor S. Multiple sclerosis animal models: a clinical and histopathological perspective. Brain Pathol 2017;27:123-37.
[4] Faissner S, Gold R. Efficacy and Safety of the Newer Multiple Sclerosis Drugs Approved Since 2010. CNS Drugs 2018;32:269-87.
[5] Franklin RJM, Ffrench-Constant C. Regenerating CNS myelin - from mechanisms to experimental medicines. Nat Rev Neurosci 2017;18:753-69.
[6] Patani R, Balaratnam M, Vora A, Reynolds R. Remyelination can be extensive in multiple sclerosis despite a long disease course. Neuropathol Appl Neurobiol 2007;33:277-87.
[7] Patrikios P, Stadelmann C, Kutzelnigg A, Rauschka H, Schmidbauer M, Laursen H, Sorensen PS, Bruck W, Lucchinetti C, Lassmann H. Remyelination is extensive in a subset of multiple sclerosis patients. Brain 2006;129:3165-72.
[8] Boyd A, Zhang H, Williams A. Insufficient OPC migration into demyelinated lesions is a cause of poor remyelination in MS and mouse models. Acta Neuropathol 2013;125:841-59.
[9] Woodruff RH, Fruttiger M, Richardson WD, Franklin RJ. Platelet-derived growth factor regulates oligodendrocyte progenitor numbers in adult CNS and their response following CNS demyelination. Mol Cell Neurosci 2004;25:252-62.
[10] Zhang H, Jarjour AA, Boyd A, Williams A. Central nervous system remyelination in culture--a tool for multiple sclerosis research. Exp Neurol 2011;230:138-48.
[11] Birgbauer E, Rao TS, Webb M. Lysolecithin induces demyelination in vitro in a cerebellar slice culture system. J Neurosci Res 2004;78:157-66.
[12] Huang JK, Jarjour AA, Nait Oumesmar B, Kerninon C, Williams A, Krezel W, Kagechika H, Bauer J, Zhao C, Baron-Van Evercooren A, Chambon P, Ffrench-Constant C, Franklin RJM. Retinoid X receptor gamma signaling accelerates CNS remyelination. Nat Neurosci 2011;14:45-53.
[13] Yuen TJ, Johnson KR, Miron VE, Zhao C, Quandt J, Harrisingh MC, Swire M, Williams A, McFarland HF, Franklin RJ, Ffrench-Constant C. Identification of endothelin 2 as an inflammatory factor that promotes central nervous system remyelination. Brain 2013;136:1035-47.
[14] Mi S, Miller RH, Tang W, Lee X, Hu B, Wu W, Zhang Y, Shields CB, Zhang Y, Miklasz S, Shea D, Mason J, Franklin RJ, Ji B, Shao Z, Chedotal A, Bernard F, Roulois A, Xu J, Jung V, Pepinsky B. Promotion of central nervous system remyelination by induced differentiation of oligodendrocyte precursor cells. Ann Neurol 2009;65:304-15.
[15] Lucchinetti C, Bruck W, Parisi J, Scheithauer B, Rodriguez M, Lassmann H. A quantitative analysis of oligodendrocytes in multiple sclerosis lesions. A study of 113 cases. Brain 1999;122 (Pt 12):2279-95.
[16] Bin JM, Rajasekharan S, Kuhlmann T, Hanes I, Marcal N, Han D, Rodrigues SP, Leong SY, Newcombe J, Antel JP, Kennedy TE. Full-length and fragmented netrin-1 in multiple sclerosis plaques are inhibitors of oligodendrocyte precursor cell migration. Am J Pathol 2013;183:673-80.
[17] Tepavcevic V, Kerninon C, Aigrot MS, Meppiel E, Mozafari S, Arnould-Laurent R, Ravassard P, Kennedy TE, Nait-Oumesmar B, Lubetzki C. Early netrin-1 expression impairs central nervous system remyelination. Ann Neurol 2014;76:252-68.
[18] Buwalda SJ, Vermonden T, Hennink WE. Hydrogels for Therapeutic Delivery: Current Developments and Future Directions. Biomacromolecules 2017;18:316-30.

[19] Browning MB, Cereceres SN, Luong PT, Cosgriff-Hernandez EM. Determination of the in vivo degradation mechanism of PEGDA hydrogels. J Biomed Mater Res A 2014;102:4244-51.
[20] Ingavle GC, Gehrke SH, Detamore MS. The bioactivity of agarose-PEGDA interpenetrating network hydrogels with covalently immobilized RGD peptides and physically entrapped aggrecan. Biomaterials 2014;35:3558-70.
[21] Robert A. Scott NAP. Highly crosslinked, PEG-containing copolymers for sustained solute delivery. Biomaterials 1999;20:1371-80.

[22] Liu Z, Wang L, Bao C, Li X, Cao L, Dai K, Zhu L. Cross-linked PEG via degradable phosphate ester bond: synthesis, water-swelling, and application as drug carrier. Biomacromolecules 2011;12:2389-95.
[23] Hoffman AS. Hydrogels for biomedical applications. Advanced Drug Delivery Reviews 2012;64:18-23.
[24] Hoare TR, Kohane DS. Hydrogels in drug delivery: Progress and challenges. Polymer 2008;49:1993-2007.
[25] Wu J, Zhao Q, Sun J, Zhou Q. Preparation of poly(ethylene glycol) aligned porous cryogels using a unidirectional freezing technique. Soft Matter 2012;8:3620.
[26] Lozinsky VI, Galaev IY, Plieva FM, Savina IN, Jungvid H, Mattiasson B. Polymeric cryogels as promising materials of biotechnological interest. Trends Biotechnol 2003;21:445-51.
[27] Dragan ES, Apopei Loghin DF, Cocarta A-I, Doroftei M. Multi-stimuli-responsive semi-IPN cryogels with native and anionic potato starch entrapped in poly(N,N-dimethylaminoethyl methacrylate) matrix and their potential in drug delivery. Reactive and Functional Polymers 2016;105:66-77.
[28] de Lima GG, Traon F, Moal E, Canillas M, Rodriguez MA, McCarthy HO, Dunne N, Devine DM, Nugent MJD. Composite cryogels for dual drug delivery and enhanced mechanical properties. Polymer Composites 2018;39:E210-E20.
[29] Koshy ST, Ferrante TC, Lewin SA, Mooney DJ. Injectable, porous, and cell-responsive gelatin cryogels. Biomaterials 2014;35:2477-87.
[30] Koshy ST, Zhang DKY, Grolman JM, Stafford AG, Mooney DJ. Injectable nanocomposite cryogels for versatile protein drug delivery. Acta Biomater 2018;65:36-43.
[31] Moran MB, Martin GC. The Laser Raman Spectrum of Polyethylene Glycol Dimethacrylate). Journal of Macromolecular Science: Part A - Chemistry 2006;19:611-8.
[32] González-Henríquez CM, Pizarro GdC, Sarabia-Vallejos MA, Terraza CA, López-Cabaña ZE. In situ-preparation and characterization of silver-HEMA/PEGDA hydrogel matrix nanocomposites: Silver inclusion studies into hydrogel matrix. Arabian Journal of Chemistry 2014.
[33] Welzel PB, Grimmer M, Renneberg C, Naujox L, Zschoche S, Freudenberg U, Werner C. Macroporous starPEG-heparin cryogels. Biomacromolecules 2012;13:2349-58.
[34] Sharma A, Bhat S, Nayak V, Kumar A. Efficacy of supermacroporous poly(ethylene glycol)-gelatin cryogel matrix for soft tissue engineering applications. Mater Sci Eng C Mater Biol Appl 2015;47:298-312.
[35] Blakemore W, Franklin R. Remyelination in experimental models of toxin-induced demyelination. Advances in Multiple Sclerosis and Experimental Demyelinating Diseases: Springer; 2008. p. 193-212.
[36] Bjugstad KB, Lampe K, Kern DS, Mahoney M. Biocompatibility of poly(ethylene glycol)-based hydrogels in the brain: An analysis of the glial response across space and time. Journal of Biomedical Materials Research Part A 2010;95A:79-91.

[37] Borg DJ, Welzel PB, Grimmer M, Friedrichs J, Weigelt M, Wilhelm C, Prewitz M, Stißel A, Hommel A, Kurth T, Freudenberg U, Bonifacio E, Werner C. Macroporous biohybrid cryogels for co-housing pancreatic islets with mesenchymal stromal cells. Acta Biomaterialia 2016;44:178-87.
[38] Newland B, Welzel PB, Newland H, Renneberg C, Kolar P, Tsurkan M, Rosser A, Freudenberg U, Werner C. Tackling cell transplantation anoikis: An injectable, shape memory cryogel microcarrier platform material for stem cell and neuronal cell growth. Small 2015;11:5047-53.
[39] Koshy ST, Zhang DKY, Grolman JM, Stafford AG, Mooney DJ. Injectable nanocomposite cryogels for versatile protein drug delivery. Acta Biomaterialia 2018;65:36-43.
[40] Lagumersindez-Denis N, Wrzos C, Mack M, Winkler A, van der Meer F, Reinert MC, Hollasch H, Flach A, Bruhl H, Cullen E, Schlumbohm C, Fuchs E, Linington C, Barrantes-Freer A, Metz I, Wegner C, Liebetanz D, Prinz M, Bruck W, Stadelmann C, Nessler S. Differential contribution of immune effector mechanisms to cortical demyelination in multiple sclerosis. Acta Neuropathol 2017;134:15-34.
[41] Wegner C, Stadelmann C. Gray matter pathology and multiple sclerosis. Curr Neurol Neurosci Rep 2009;9:399-404.
[42] De Stefano N, Narayanan S, Francis GS, Arnaoutelis R, Tartaglia MC, Antel JP, Matthews PM, Arnold DL. Evidence of axonal damage in the early stages of multiple sclerosis and its relevance to disability. Arch Neurol 2001;58:65-70.
[43] Fisniku LK, Chard DT, Jackson JS, Anderson VM, Altmann DR, Miszkiel KA, Thompson AJ, Miller DH. Gray matter atrophy is related to long-term disability in multiple sclerosis. Ann Neurol 2008;64:247-54.
[44] Filippi M, Preziosa P, Copetti M, Riccitelli G, Horsfield MA, Martinelli V, Comi G, Rocca MA. Gray matter damage predicts the accumulation of disability 13 years later in MS. Neurology 2013;81:1759-67.

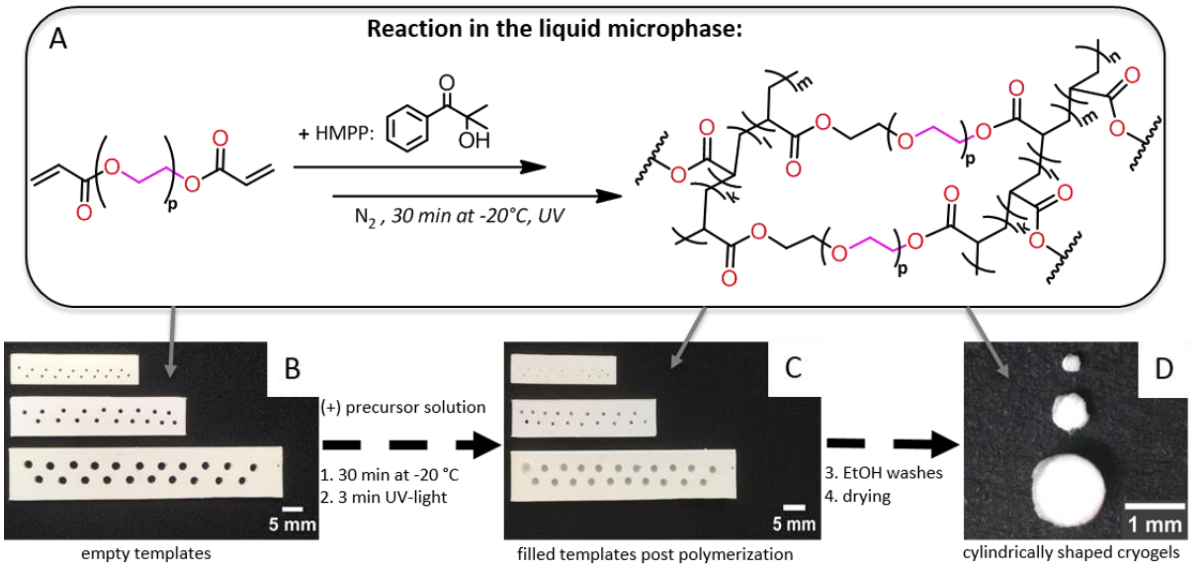

Figure 1. Schematic depiction of the preparation process of cylindrical PEGDA cryogels.

(A) Synthesis of the PEGDA cryogel network via free radical photo-polymerization reaction within the liquid non-frozen microphase. (B) Empty polystyrene template sheets with cavities for the precursor solution. (C) Cryogel filled polystyrene sheets post polymerization. (D) Washed and dried cylindrical cryogels, removed from the polystyrene sheet cavities.

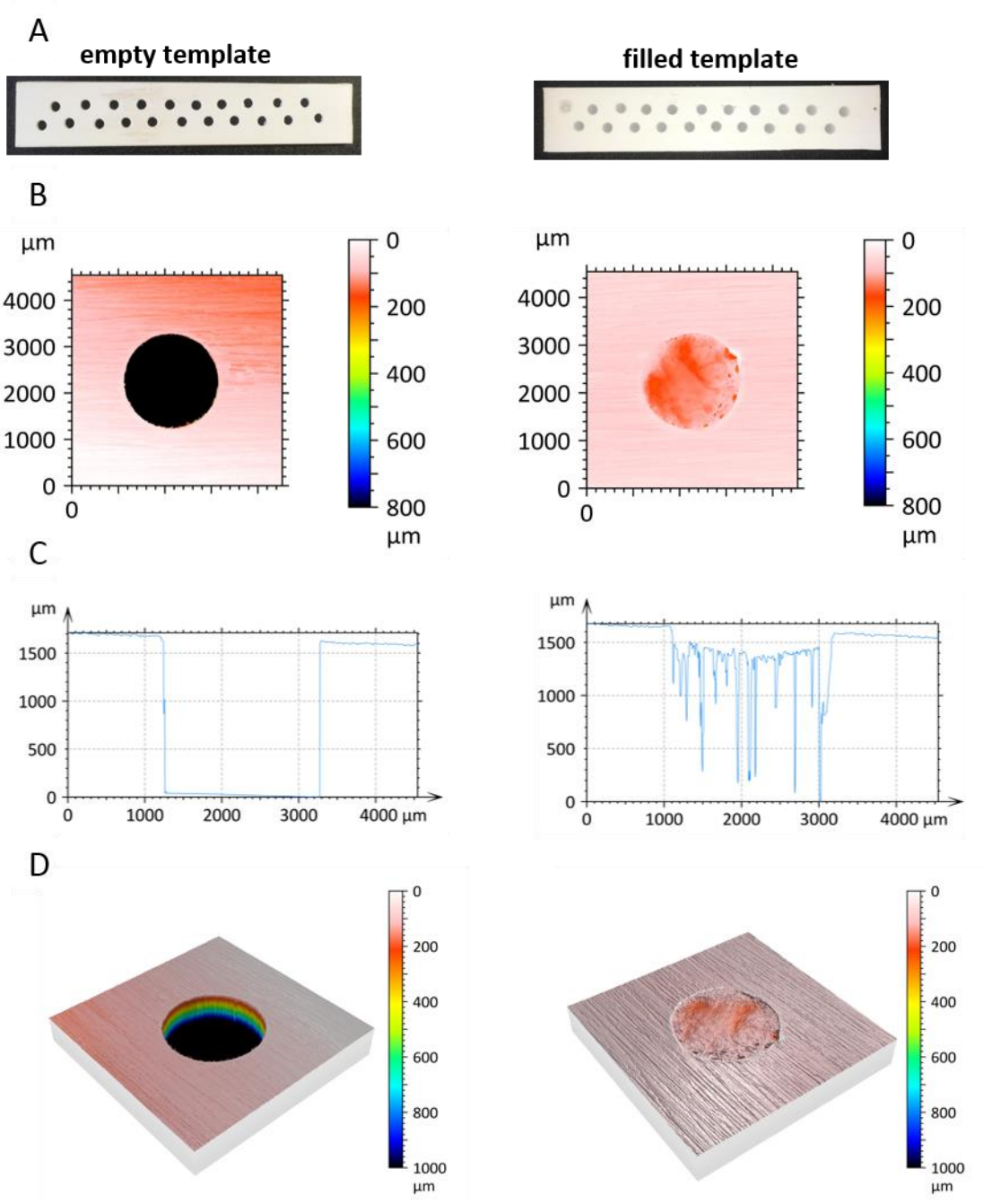

Figure 2. Multi-pinhole confocal microscopy analysis of the polystyrene templates. (A) Photo images of empty and filled 2 mm diameter cryogel template. (B) 2D multi-pinhole confocal microscopy analysis of the 2 mm diameter polystyrene template empty and filled post polymerization. (C) Profile analysis of the empty and filled 2 mm templates polystyrene sheets post polymerization. (D) 3D multi-pinhole confocal microscopy analysis of the 2 mm diameter polystyrene template empty and filled post polymerization.

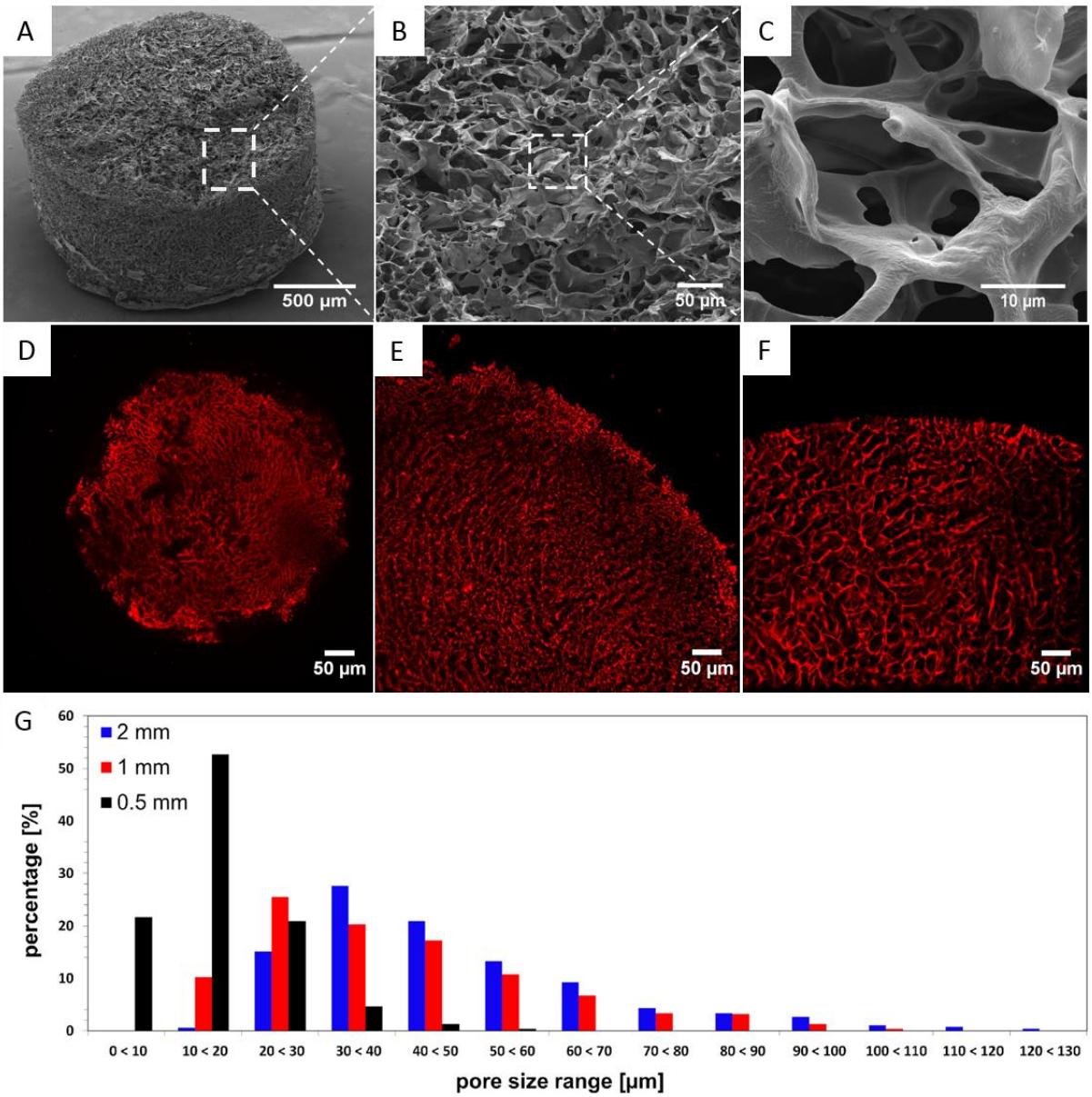

Figure 3. Scanning electron microscopy and confocal laser fluorescence microscopy analysis of cylindrical PEGDA cryogel scaffolds.

(A-C) Representative scanning electron microscopy images of a 2 mm cylindrical PEGDA cryogel scaffold in its dehydrated state shows its porous nature. (D-F) Confocal laser fluorescence microscopy analysis of ATTO 647 maleimide labelled cylindrical cryogel scaffolds with 0.5 mm (D), 1 mm (E), and 2 mm diameter (F) showing the high precision control over scaffold dimensions. (G) Pore size distribution of 0.5 mm, 1 mm and 2 mm diameter cryogels (swollen in PBS).

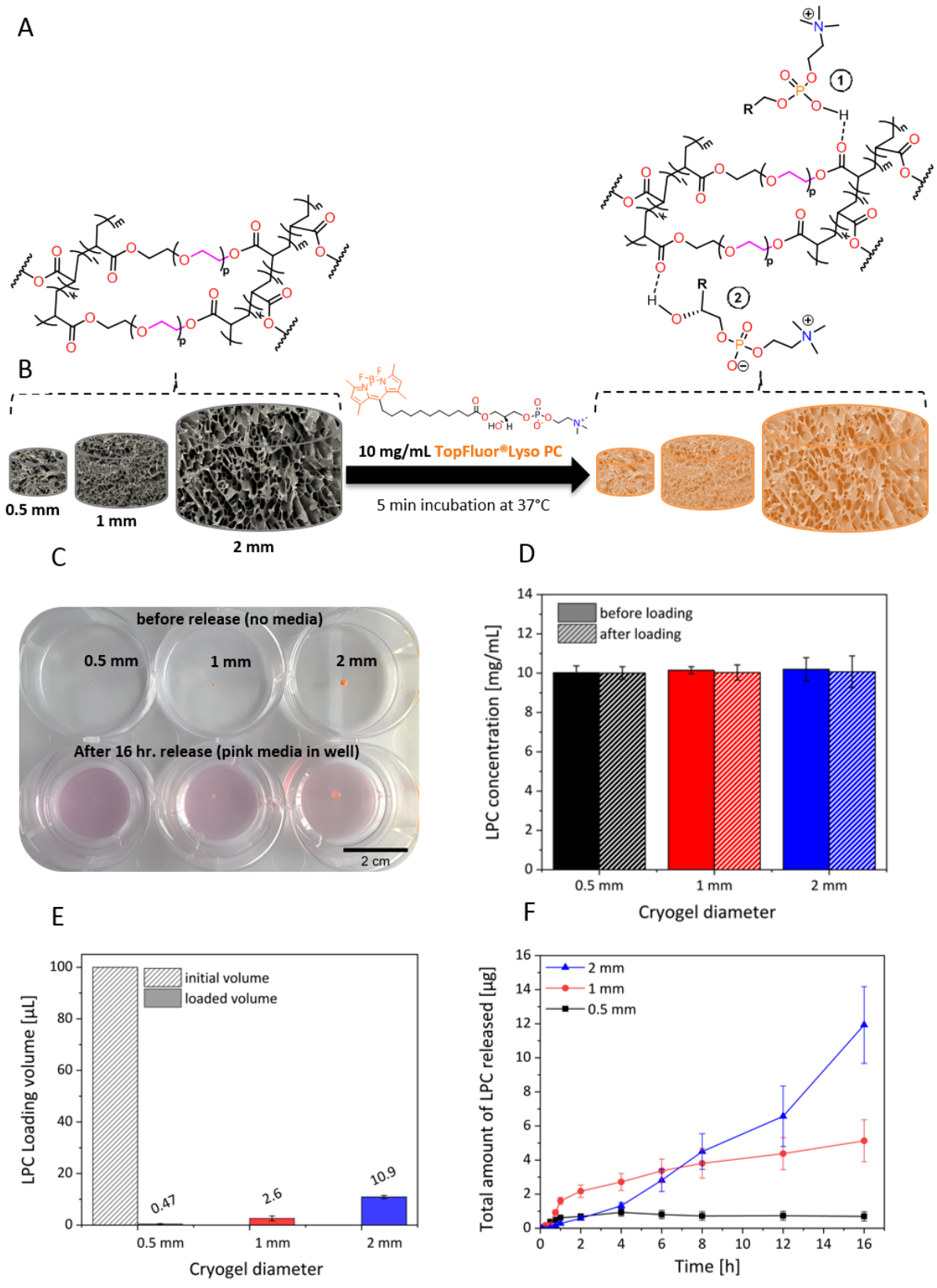

Figure 4. **An illustration of the molecular interactions between the PEGDA cryogel network and the fluorescently labelled LPC** (A): (1) Hydrogen bond interactions between the phosphonate group of LPC and the carbonyl functionality of PEGDA (2) Hydrogen bond interactions between the hydroxide group of LPC and the carbonyl

functionality of PEGDA. (B-C) PEGDA cryogel cylinders placed in the 6-well inserts in empty wells (top row) and wells containing media (bottom row). The cryogels turned into an orange colour after incubation in the fluorescently labelled LPC solution (top row). After 16 hours of release, the cryogels are discoloured (bottom row). (D-F) Loading and release properties of LPC from the 0.5-2 mm diameter PEGDA cryogels. (D) shows that the LPC concentration was completely unaffected by the cryogel loading process. (E) shows the loaded volume of the LPC solution to the different sized PEGDA cryogels after the soaking procedure. The loading volume capacity increases with the cryogel size. (F) shows a slow release profile with a low amount released from the cryogels over a period of 16 hours. (n = 4) (error bars represent the cumulative value of the standard error).

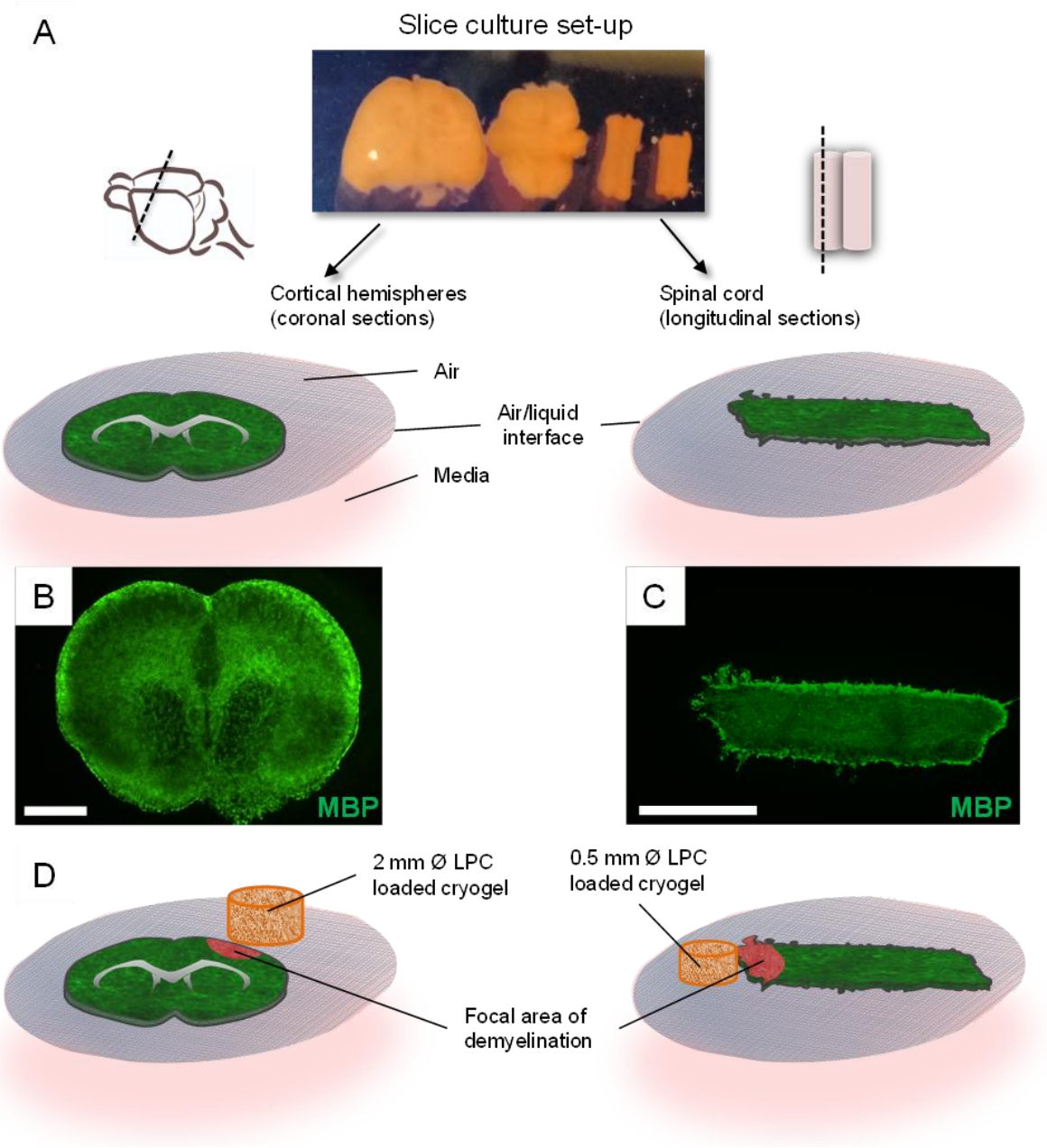

Figure 5: Technical information for slice cultures ex vivo

(A) Diagram of angle of cutting of spinal cord and cortical hemispheres for cultures on membrane inserts in culture wells. (B and C) micrographs of cultured brain slice (B) and spinal cord slice (C) stained with an antibody against myelin basic protein (MBP) in green (scale bars represent 1mm). (D) Schematic representations of the placement of the cryogels adjacent to the tissue slices, showing their position on the insert relative to the tissue.

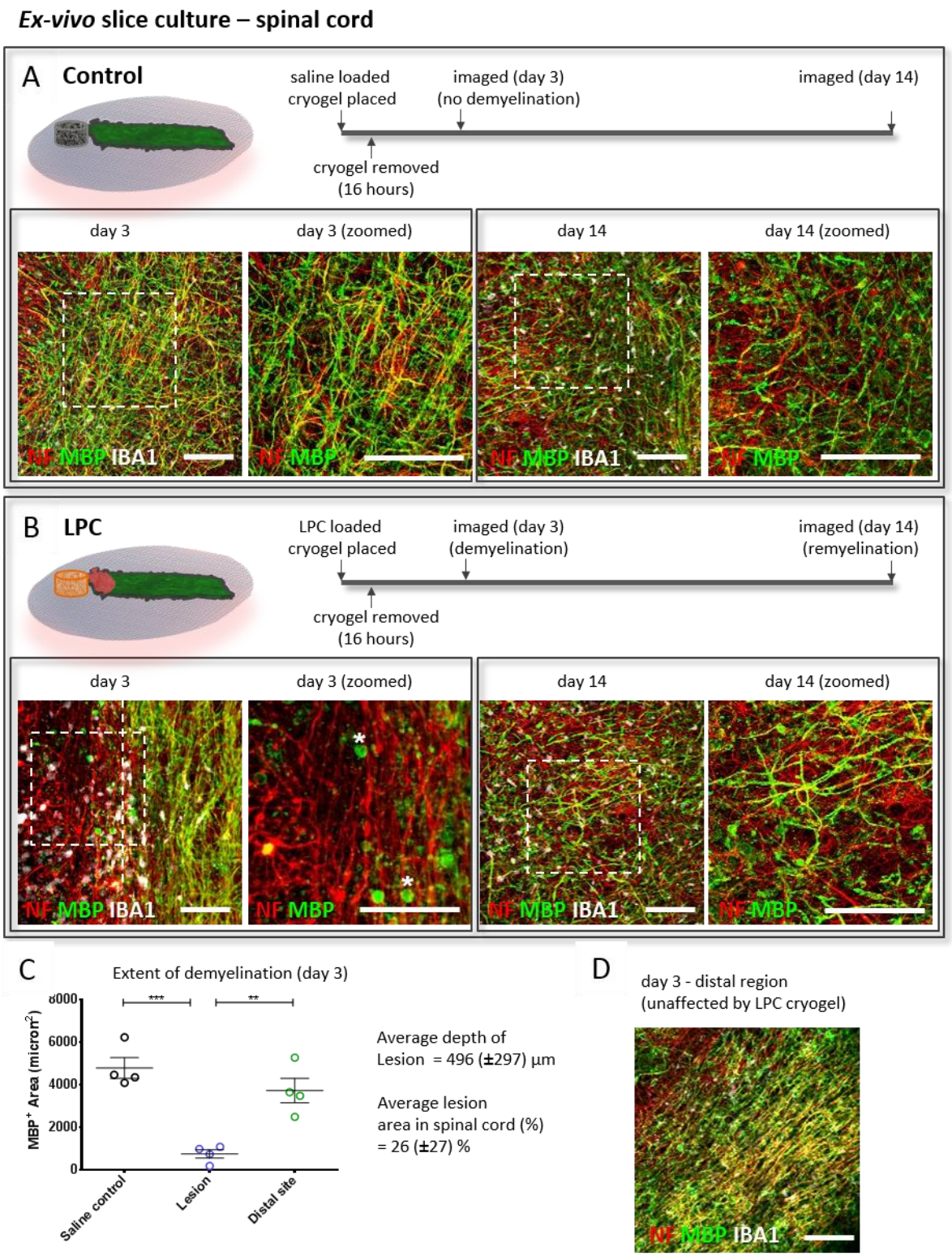

Figure 6: LPC loaded cryogels create a focal lesion in spinal cord ex-vivo slice cultures.

(A) Schematic representation of a saline loaded cryogel (control condition) placed next to a spinal cord slice with corresponding timeline of study procedure. Immunohistochemistry of horizontal sections for MBP (green), NF (red), and IBA1

(white) for brain slices cultured in the control condition. Higher magnification images (zoomed) are taken from the regions marked by the dashed box, with IBA1 omitted for clarity. No demyelination occurs in this condition (scale bars represent 100 μm). **(B)** Schematic representation of a LPC loaded cryogel (test condition) placed next to a spinal cord slice with corresponding timeline. Micrographs taken at day 3 show extensive demyelination (lesion border shown by dashed line) with myelin debris marked with an asterisk in the zoomed images. As with the cortical sections, by day 14, the presence of increased numbers of myelinated axons is clear and IBA1+ microglial cells are more evenly distributed (not clustered around the lesion site), showing that spontaneous remyelination has occurred (scale bars represent 100 μm). **(C)** Quantification of the extent of demyelination at day 3. The region of the lesion shows a significant reduction in the area of MBP signalling compared to the saline control, the perilesion and distal to the lesion. Each point represents data from one animal. Data are shown as mean ±SEM. One-way ANOVA with Tukey post-hoc test (*$P<0.05$, ** $P<0.01$, *** $P<0.001$). **(D)** Quantification of the extent of remyelination at day 14. The area of MBP+ signal was measured. The lesion area shows similar MBP signalling when compared to the saline control and the distal area. Each point represents data from one animal. Data are shown as mean ±SEM. One-way ANOVA with Tukey post-hoc test ($P=0.0791$ n.s.: non-significant).

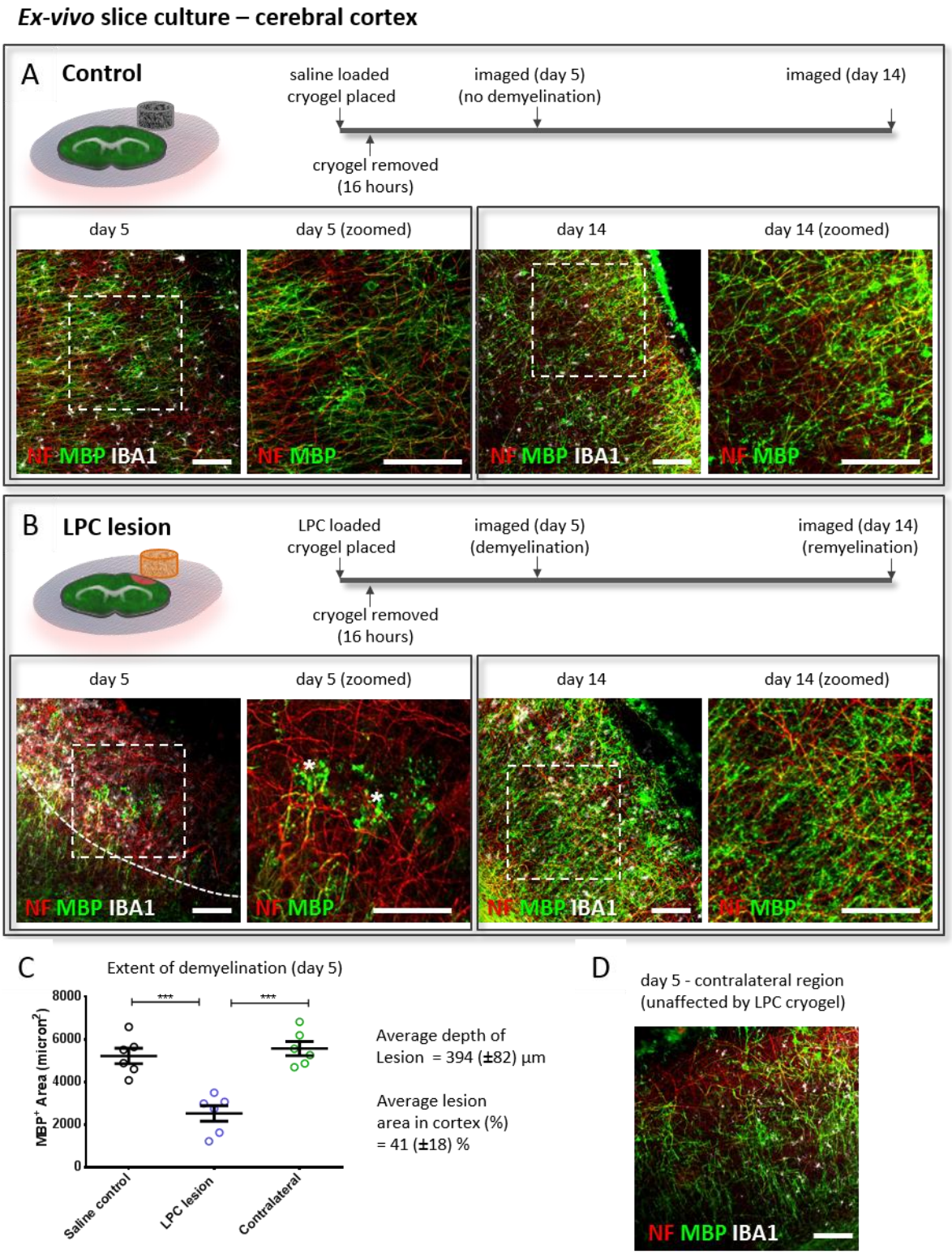

Figure 7: Focal lesion in cortical hemisphere cultures in *ex vivo* slice cultures created by LPC loaded cryogels

(A) Schematic representation of a saline loaded cryogel (control condition) placed next to a cortical brain slice with corresponding timeline of study procedure. Immunohistochemistry of coronal sections for MBP (green), NF (red), and IBA1 (white)

for brain slices cultured in the control condition. Higher magnification images (zoomed) are taken from the regions marked by the dashed box, with IBA1 omitted for clarity. No demyelination occurs in this condition (scale bars represent 100 μm). **(B)** Schematic representation of a LPC loaded cryogel (test condition) placed next to a cortical brain slice with corresponding timeline. Micrographs taken at day 5 show extensive demyelination (lesion border shown by dashed line) with myelin debris marked with an asterisk in the zoomed images. By day 14 the presence of increased numbers of myelinated axons is clear and IBA1 microglial cells are more evenly distributed, showing that spontaneous remyelination has occurred (scale bars represent 100 μm). **(C)** Quantification of the extent of demyelination at day 5. The area of MBP+ signal was measured. The lesion area shows a significant reduction of MBP signalling compared to the saline control, the perilesion and contralateral hemisphere. Each point represents data from one animal. Data are shown as mean ±SEM. One-way ANOVA with Tukey post-hoc test (*P<0.05, **P<0.01, ***P<0.001,****P<0.0001). **(D)** Quantification of the extent of remyelination at day 14. The area of MBP+ signal was measured. The lesion area shows similar MBP signalling when compared to the saline control and the contralateral hemisphere. Each point represents data from one animal. Data are shown as mean ±SEM. One-way ANOVA with Tukey post-hoc test (P=0.7739 n.s.: non-significant).

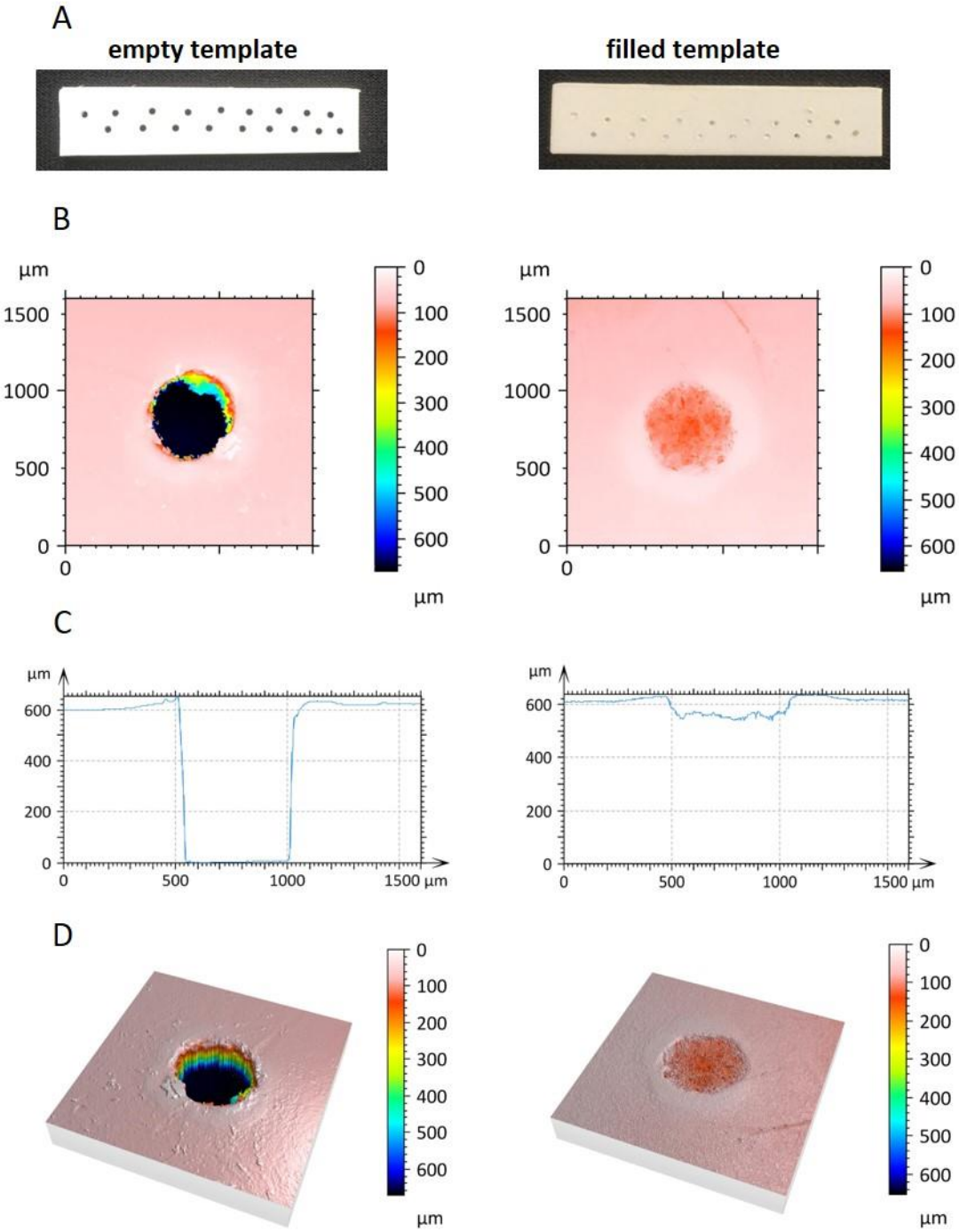

Figure S1. Multi-pinhole confocal microscopy analysis of the polystyrene templates.

(A) Photo images of empty and filled 0.5 mm diameter cryogel template. (B) 2D multi-pinhole confocal microscopy analysis of the 0.5 mm diameter polystyrene template empty and filled post polymerization. (C) Profile analysis of the empty and filled 0.5 mm templates polystyrene sheets post polymerization. (D) 3D multi-pinhole confocal

microscopy analysis of the 0.5 mm diameter polystyrene template empty and filled post polymerization.

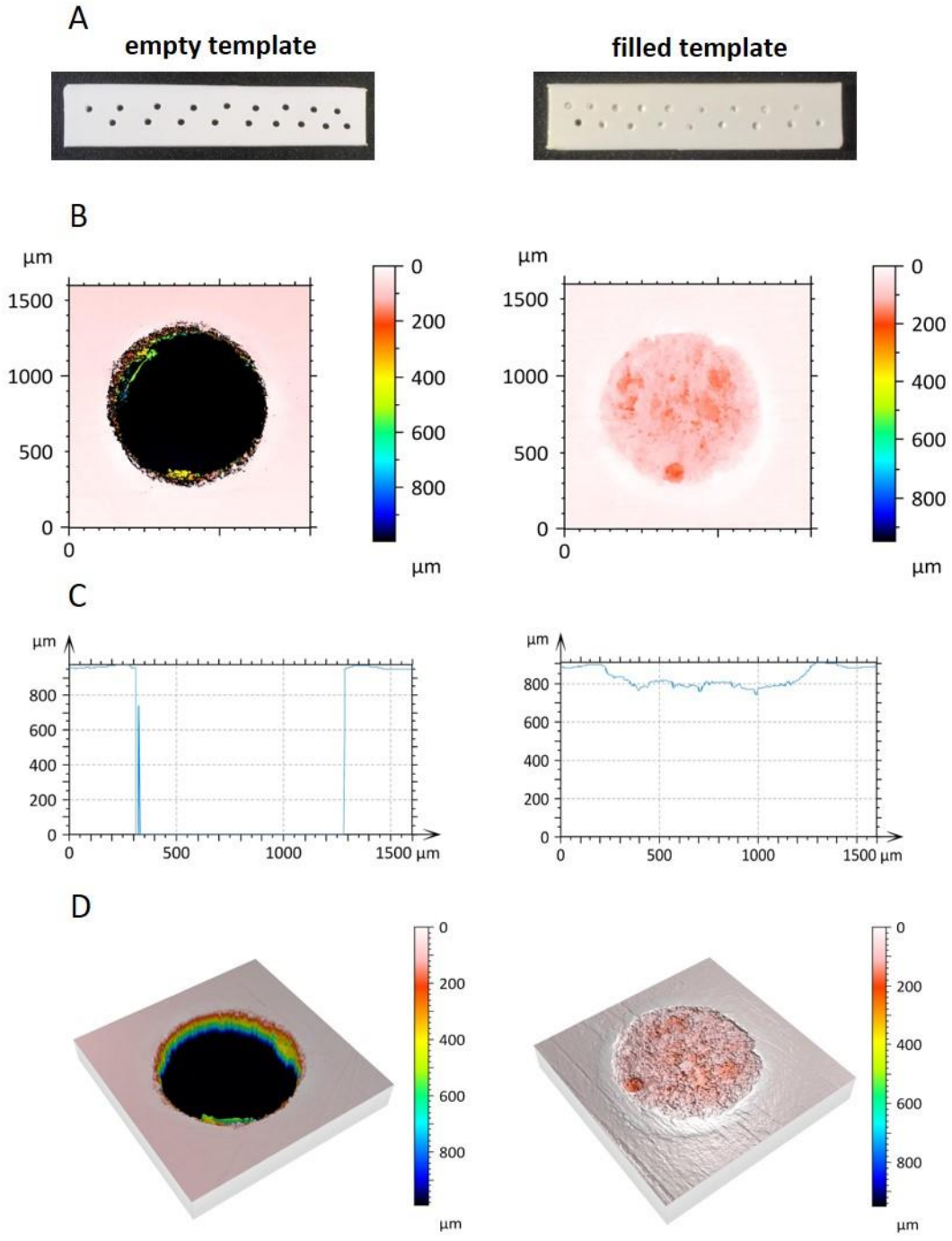

Figure S2. Multi-pinhole confocal microscopy analysis of the polystyrene templates.

(A) Photo images of empty and filled 1 mm diameter cryogel template. (B) 2D multi-pinhole confocal microscopy analysis of the 1 mm diameter polystyrene template empty and filled post polymerization. (C) Profile analysis of the empty and filled 1 mm templates

polystyrene sheets post polymerization. (D) 3D multi-pinhole confocal microscopy analysis of the 1 mm diameter polystyrene template empty and filled post polymerization.

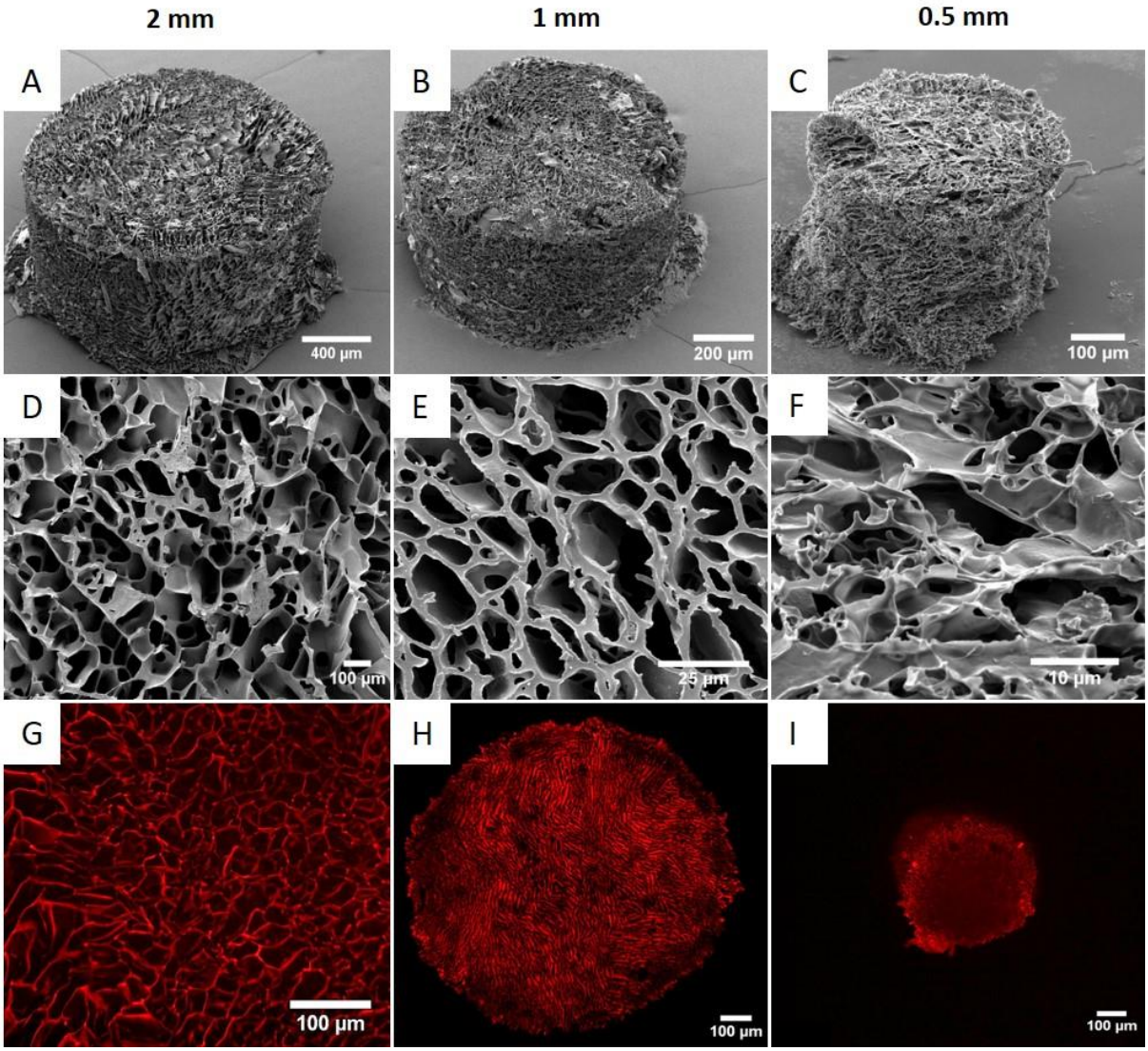

Figure S3. Scanning electron microscopy analysis of cylindrical PEGDA cryogel scaffolds confocal laser fluorescence microscopy analysis.

(A-F) Scanning electron microscopy images of cylindrical PEGDA cryogel scaffolds with 2 mm (A,D), 1 mm (B,E) and 0.5 mm (C,F) diameter its dehydrated state showing the porous nature of the scaffold. (G-I) Confocal laser fluorescence microscopy analysis of ATTO 647 maleimide labelled cylindrical cryogel scaffolds with 2 mm (G), 1 mm (H), and 0.5 mm diameter (F) showing the high precision control over scaffold dimensions.

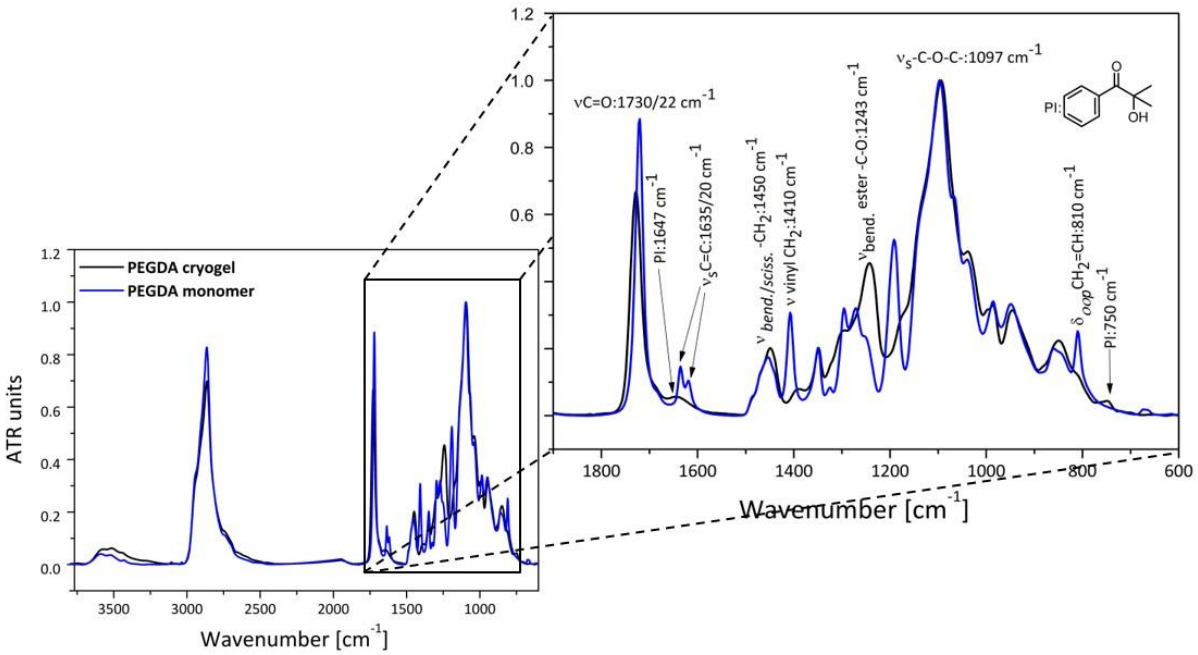

Figure S4. FTIR analysis of the cryogels in comparison to the monomer.

FTIR spectra of the non-crosslinked PEGDA monomer (**blue**) and the cylindrical shaped PEGDA cryogels (**black**), showing a complete reduction in the peak at 810 cm^{-1}, 1620-1635 cm^{-1} and 1410 cm^{-1} due to the radical photo-polymerization reaction of the acrylate.

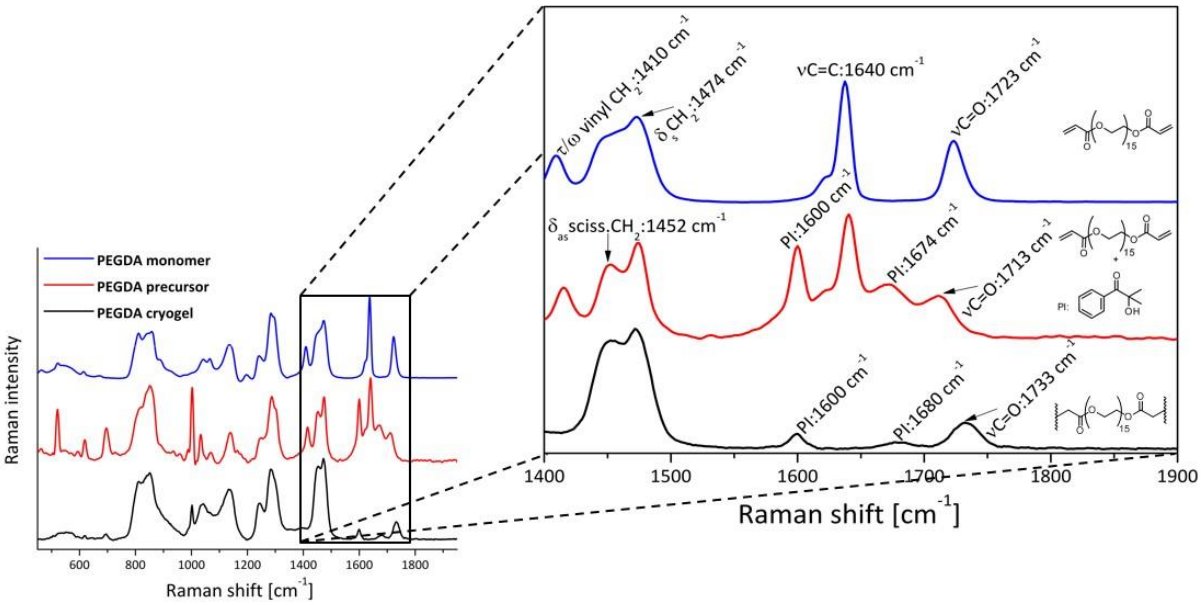

Figure S5. Raman spectra analysis of the cryogel scaffold.

Raman spectra of the non-crosslinked PEGDA monomer (blue), the precursor solution with the non-crosslinked PEGDA monomer and HMPP as the photoinitiator (red) and the cylindrical shaped PEGDA sample after photo-crosslinking and cryo-polymerization (black), showing a complete reduction in the peak at 1410 cm-1 and 1640 cm-1 (blue/red to black) because of the radical photo-polymerization reaction of the acrylate. Due to the

use of the photoinitiator HMPP, the presence of aromatic C-H and C-C vibrations (1000 cm-1, 1600 cm-1 Raman; 750 cm-1 and 1647 cm-1, FTIR) with additionally related C=O vibrations (1680 cm-1, Raman) were evident in the cryogel spectrum.

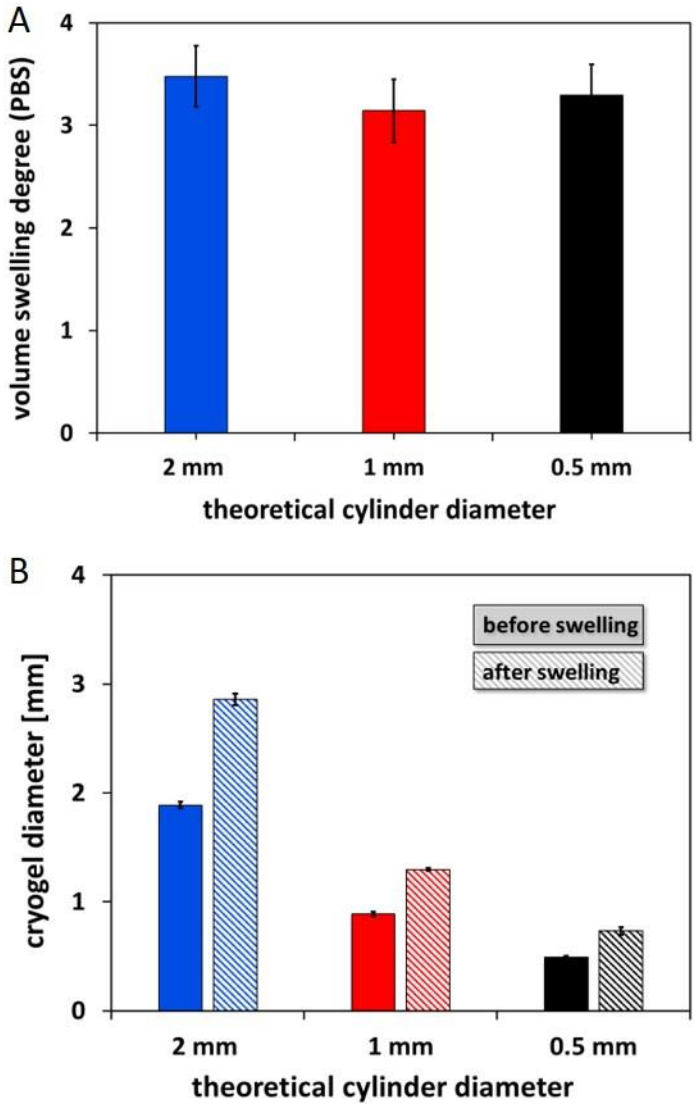

Figure S6. Swelling properties of the cylindrical PEGDA cryogels.

(A) Experimentally determined volume swelling properties of 0.5, 1 and 2 mm diameter size PEGDA cryogels in PBS at 37 °C. Data collected are presented as mean ± standard deviation (n=6). (B) Comparison of theoretical and experimentally determined diameter of the cylindrical PEGDA cryogels in PBS at 37 °C. Data collected are presented as mean ± standard deviation (n=6).

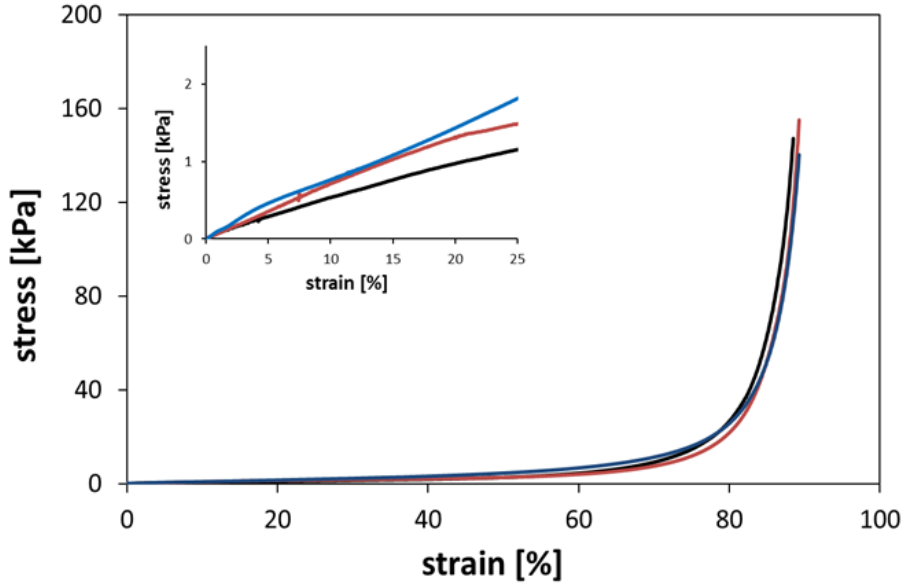

Figure S7. Compression test of the cylindrical PEGDA cryogels.

The black, red and blue curve represent an example of uniaxial compression stress-strain measurements obtained from the PEGDA cryogels (n = 10) at the rate of 1mm/min.

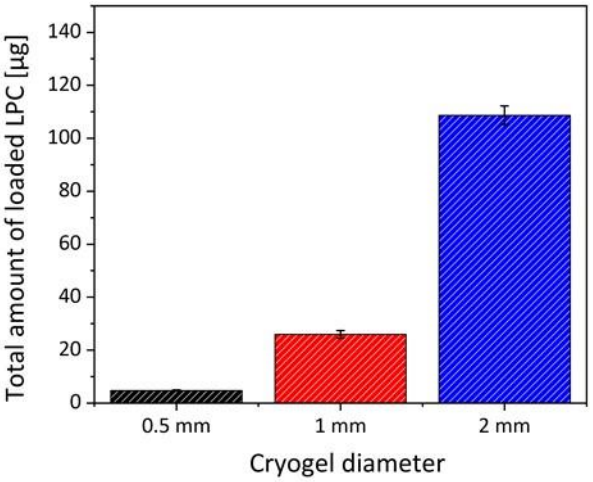

Figure S8. Loaded amount of LPC from the 0.5-2 mm diameter PEGDA cryogels. A small amount, up to a max. of 0.11 mg was loaded to the cryogel scaffold from the loading stock solution containing 10 mg in total.

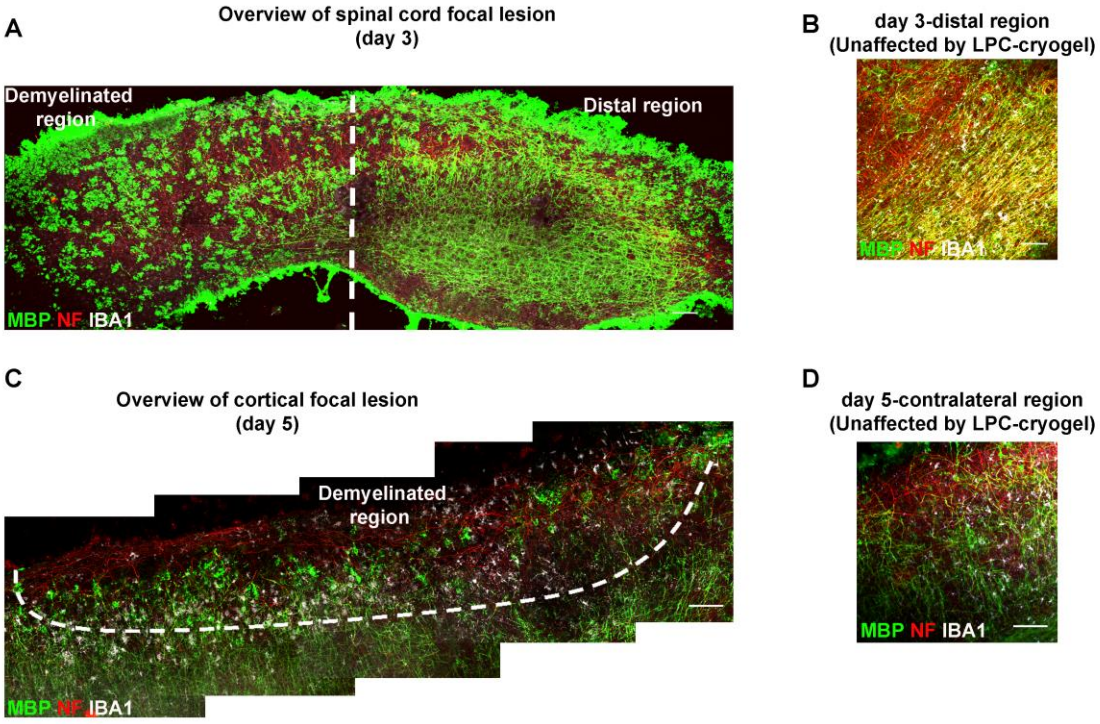

Figure S9. Tiled immunofluorescence pictures of large areas of focally demyelinated CNS tissue

(A) Slide scanner image of a focal demyelinated lesion 3 days after treatment with LPC in spinal cord. **(B)** A representative micrograph image of the spinal cord distal to the placement of the LPC loaded cryogel after 3 days, showing no LPC induced demyelination. **(C)** Tiled 20x images of a focal demyelinated lesion 5 days after treatment with LPC in a cortical slice. **(D)** A representative micrograph image of the cortex contralateral to the placement of the LPC loaded cryogel after 5 days, showing no LPC induced demyelination. In all pictures, immunofluorescence for MBP (green), axonal NF (red) and IBA1 (white) and scale bars represent 100 µm.

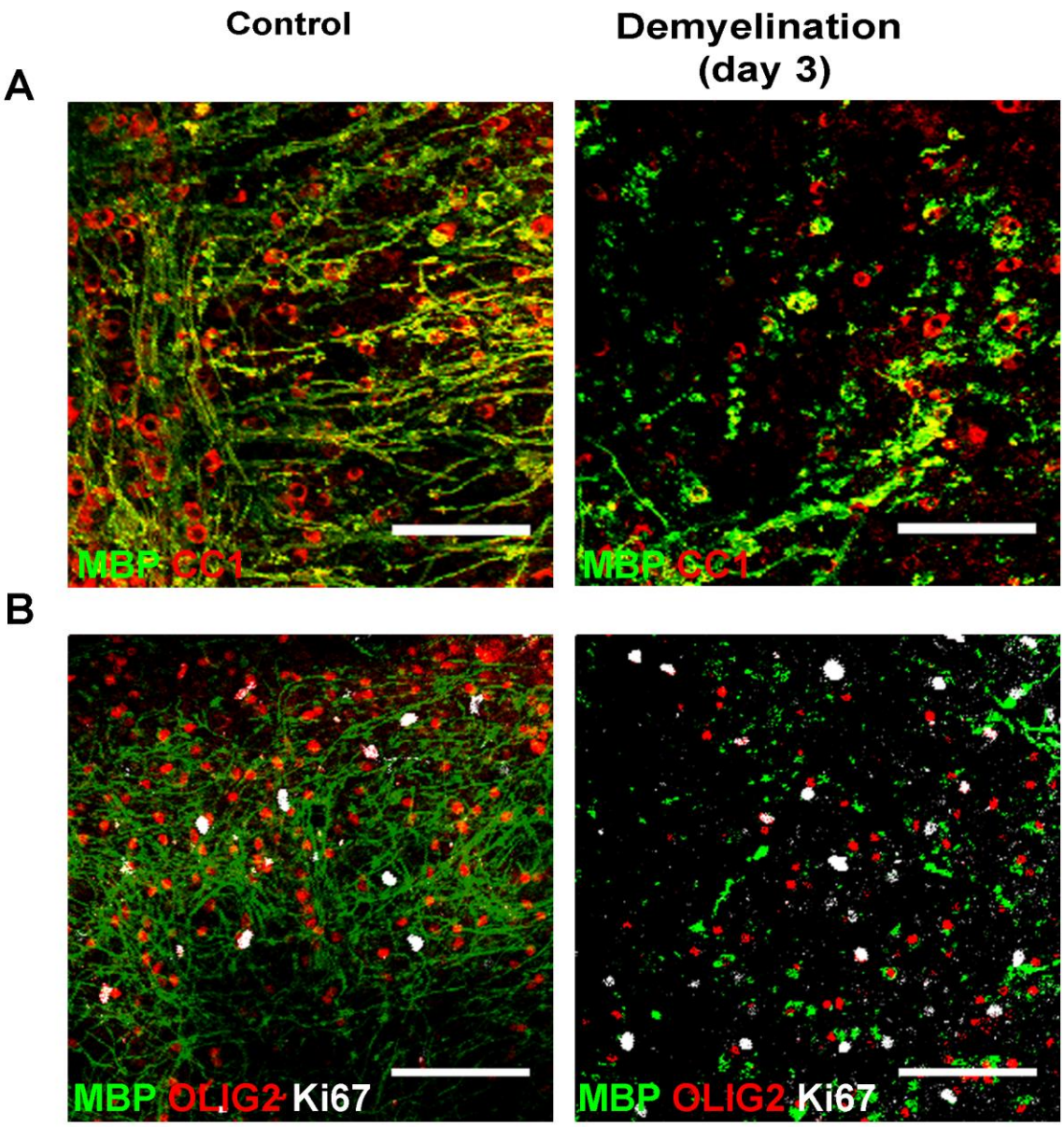

Figure S10. Examples of immunofluorescence in focally demyelinated spinal cord slice cultures

Immunofluorescence of spinal cord slices not treated (control) and within the focal demyelinated lesion at 3 days after treatment with LPC, showing **(A)** MBP (green - myelin) and CC1 (red - mature oligodendrocytes) with a reduction in both after demyelination, and **(B)** MBP (green - myelin), OLIG2 (red - oligodendroglia) and Ki67 (white – proliferating cells). Scale bars represent 100 μm.

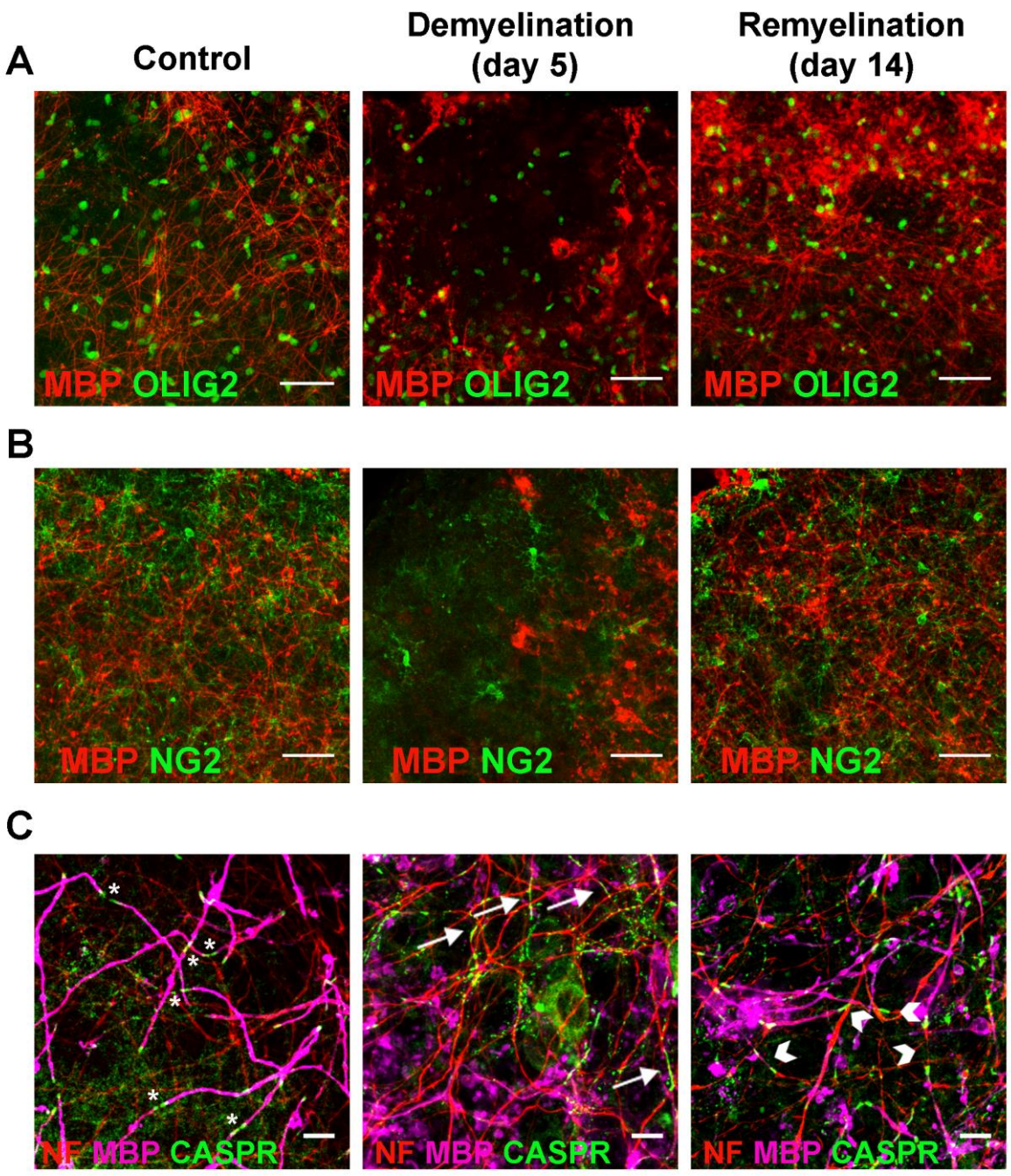

Figure S11. Examples of immunofluorescence in focally demyelinated cortical slice cultures

Immunofluorescence of coronal sections of cortical slices not treated (control), within the focal demyelinated lesion at 5 days after treatment with LPC, and after remyelination at 14 days after treatment with LPC showing **(A)** MBP (red - myelin) and OLIG2 (green - oligodendroglia) showing loss of both during demyelination and then recovery after remyelination, **(B)** MBP (red - myelin) and NG2 (green - OPCs) showing loss of both during demyelination followed by recovery after remyelination and **(C)**

MBP (magenta - myelin) NF (red - axons) and CASPR (green - paranode) showing normal clustering of CASPR protein on myelinated fibres in controls adjacent to the node of Ranvier (asterisks), but diffusion of CASPR along the axon (arrows) during demyelination, with the return of heminodal clustering upon remyelination. Scale bars represent 50 μm (A,B) and 10 μm(C).